Geophys. J. Int. (1993) **115**, 41–61

Earthquakes on the Kazerun Line in the Zagros Mountains of Iran: strike–slip faulting within a fold-and-thrust belt

Calum Baker, James Jackson and Keith Priestley
Bullard Laboratories, Madingley Rise, Cambridge CB3 OEZ, *UK*

Accepted 1993 January 18. Received 1992 December 15; in original form 1992 June 8

SUMMARY

The Kazerun Line is a transverse valley of about 200 km long that obliquely crosses the regular anticlines of the Zagros fold belt in SW Iran. At its northern end it is a clear fault which can be mapped on the surface. Anticline axes die out or bend towards this valley but do not cross it. Six moderate-sized earthquakes that occurred close the the Kazerun Line, and within a 25 km area involved right-lateral strike–slip motion parallel to the strike of the valley. They indicate that the Kazerun Line is the surface expression of a buried strike–slip fault. Slip vectors in these strike–slip earthquakes are different from those of neighbouring reverse-fault earthquakes, suggesting that the Kazerun Line accommodates some of the shortening between Arabia and central Iran by an elongation of the Zagros mountains parallel to strike. The centroid depths and the source dimensions of these earthquakes, combined with the lack of seismogenic surface faulting in the Zagros, suggest to us that all these earthquakes involve faulting in the metamorphic basement beneath the sedimentary cover. The sedimentary cover is almost certainly decoupled from the basement by several thick evaporite horizons. The seismicity of the Kazerun Line thus demonstrates how lateral interruptions to the regularity of a fold belt can arise from faulting in the basement, and not just from lateral ramps between the thrust sheets that deform the sedimentary cover.

Key words: earthquakes, Iran, strike–slip faulting, waveform modelling, Zagros.

1 INTRODUCTION

Convergence between continental plates often leads to the formation of fold-and-thrust belts. Of the many such belts that are forming today, the Zagros mountains of SW Iran is one of the simplest and most seismically active. Its formation is related to the convergence between the Arabian plate in the SW and the central plateau of Iran to the NE. At the surface, the Zagros consists of long, linear anticlinal ridges that form a series of ranges from eastern Turkey in the NW to the Strait of Hormuz in the SE, a distance of about 1200 km. The width of the belt is 200–300 km. Most of the larger earthquakes in the Zagros have fault-plane solutions that involve high-angle reverse faulting on planes that strike parallel to the local trend of the fold axes at the surface. In this respect, the deformation of the Zagros mountains is approximately 2-D, involving predominantly shortening perpendicular to strike and crustal thickening (e.g. Jackson & McKenzie 1984).

The anticlinal ridges that dominate the morphology of the Zagros are not continuous for the entire length of the belt. They are typically no longer than 100 km, and die out along strike at each end. There are several places where the ends of the anticlinal axes apparently line up, to produce sinuous valleys that are oblique to the strike of the belt, and across which the anticline axes are not continuous. The best known of these is the Kazerun Line (or Flexure), in the central Zagros (Plate 1; Figs 1 and 2), which is the subject of this paper. At its northern end it is a clear fault which can be mapped on the surface and is usually referred to as the Kazerun Fault (Manuel Berberian, personal communication). The Kazerun Line crosses the Zagros with a north–south trend, which is common also in the structures of Oman on the SW side of the Persian Gulf (Falcon 1969; Stöcklin 1974; Haynes & McQuillan 1974). Fold axes do not cross the Kazerun Line, and are generally thought to be offset in a right-lateral sense, partly because that is to be expected on a structure that is oblique in this way to the NE–SW direction of shortening (Falcon 1969; Haynes & McQuillan 1974, Colmann-Sadd 1978). The Kazerun Line seems to have influenced sedimentation in the Zagros since at least the Middle Jurassic (Koop & Stoneley 1982), which

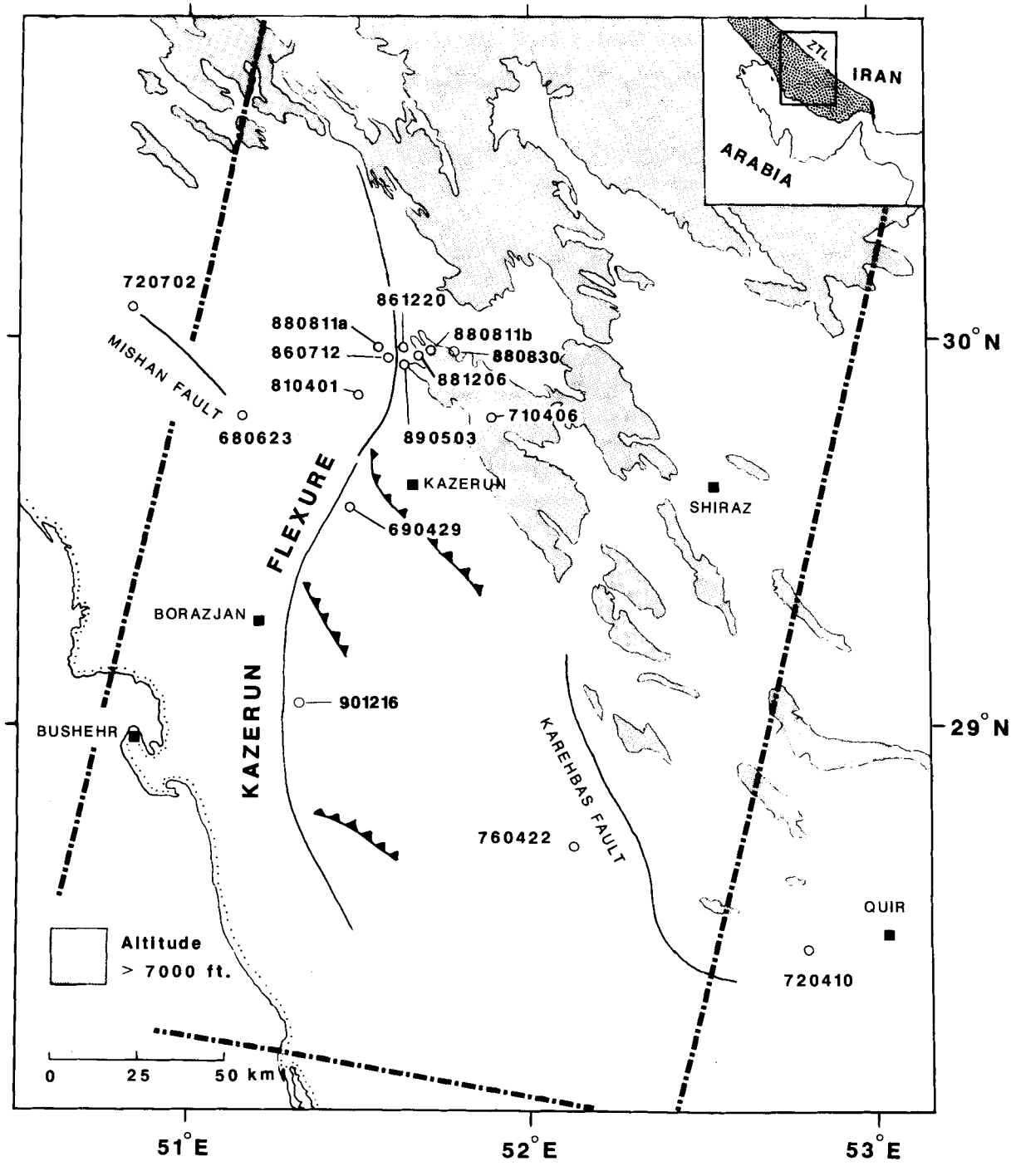

Figure 1. Location Map showing the main faults and topography in the region of the Kazerun Flexure (or Kazerun Line). The valley that marks the Kazerun Line is indicated by a thin line. The epicentres of the earthquakes discussed in this study are marked by their date (year, month, day). Principal towns are marked as black squares. The inset shows the area in relation to the Persian Gulf, with the seismic belt defining the Zagros Mountains shaded. ZTL is the Zagros Thrust Line. The dashed line defines the area shown in the satellite image in Plate 1.

suggests that it may be related to a basement structure. Basement faults of Proterozoic age in Arabia have a similar trend and are important in controlling the geometry of the hydrocarbon structures found there.

Structures that are transverse or oblique to the strike of fold-and-thrust belts, and which offset the fold axes, are not especially rare. Dahlstrom (1970) and Boyer & Elliott (1982) describe transverse structures in the Appalachians and Canadian Rocky Mountains that are interpreted as lateral ramps on thrust faults which are contained within the deforming sedimentary cover. The deformation (which is no longer active) in these cases is thought to be 'thin-skinned', and does not involve the shortening of the basement directly beneath the sedimentary cover. In the Tien Shan mountains

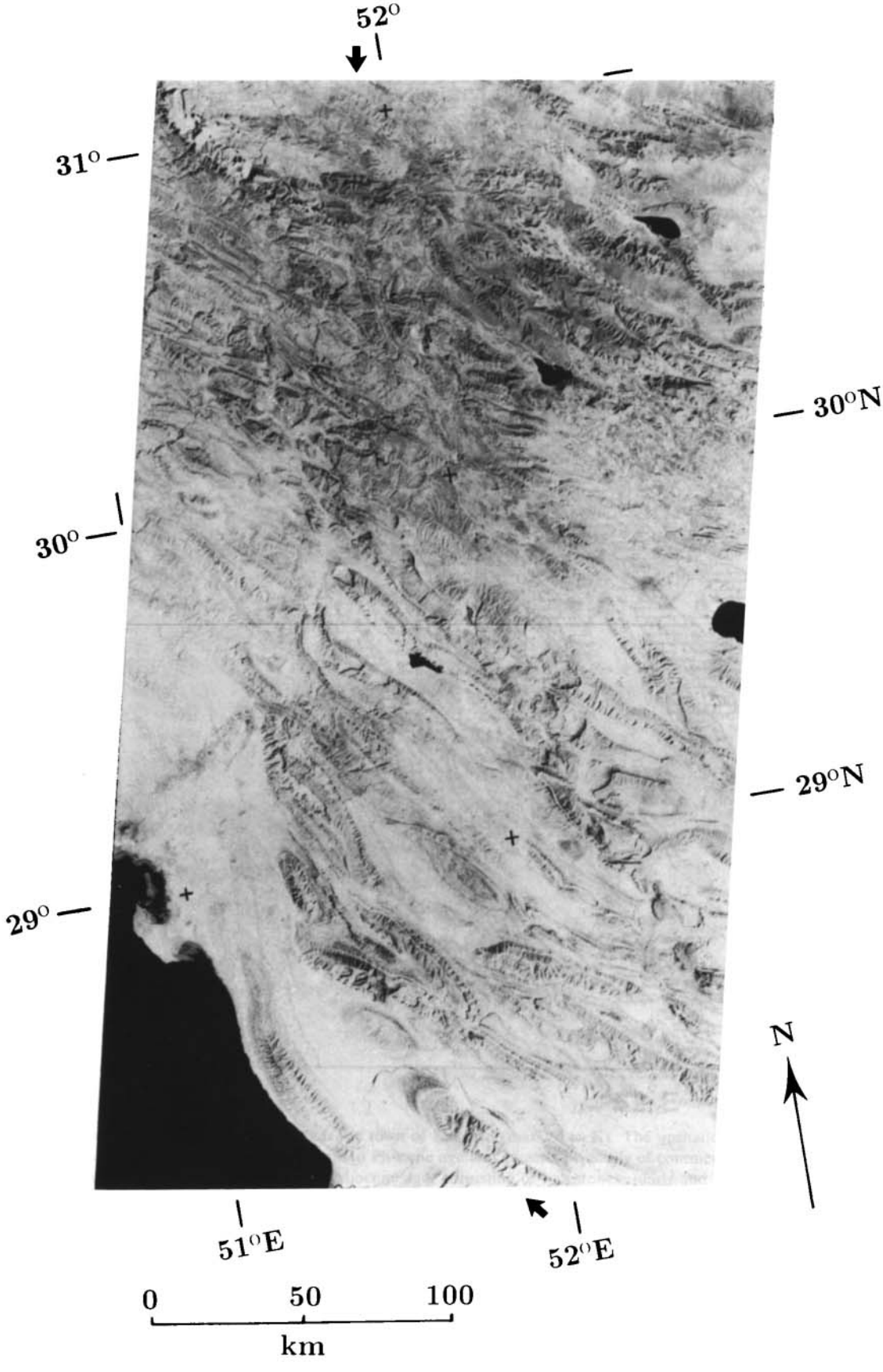

Plate 1. *Landsat 4* image of the region around the Kazerun Line. The main features and earthquake locations are shown in Fig. 1. Note how the anticline ridges do not cross the line and how they are apparently deflected as they approach it.

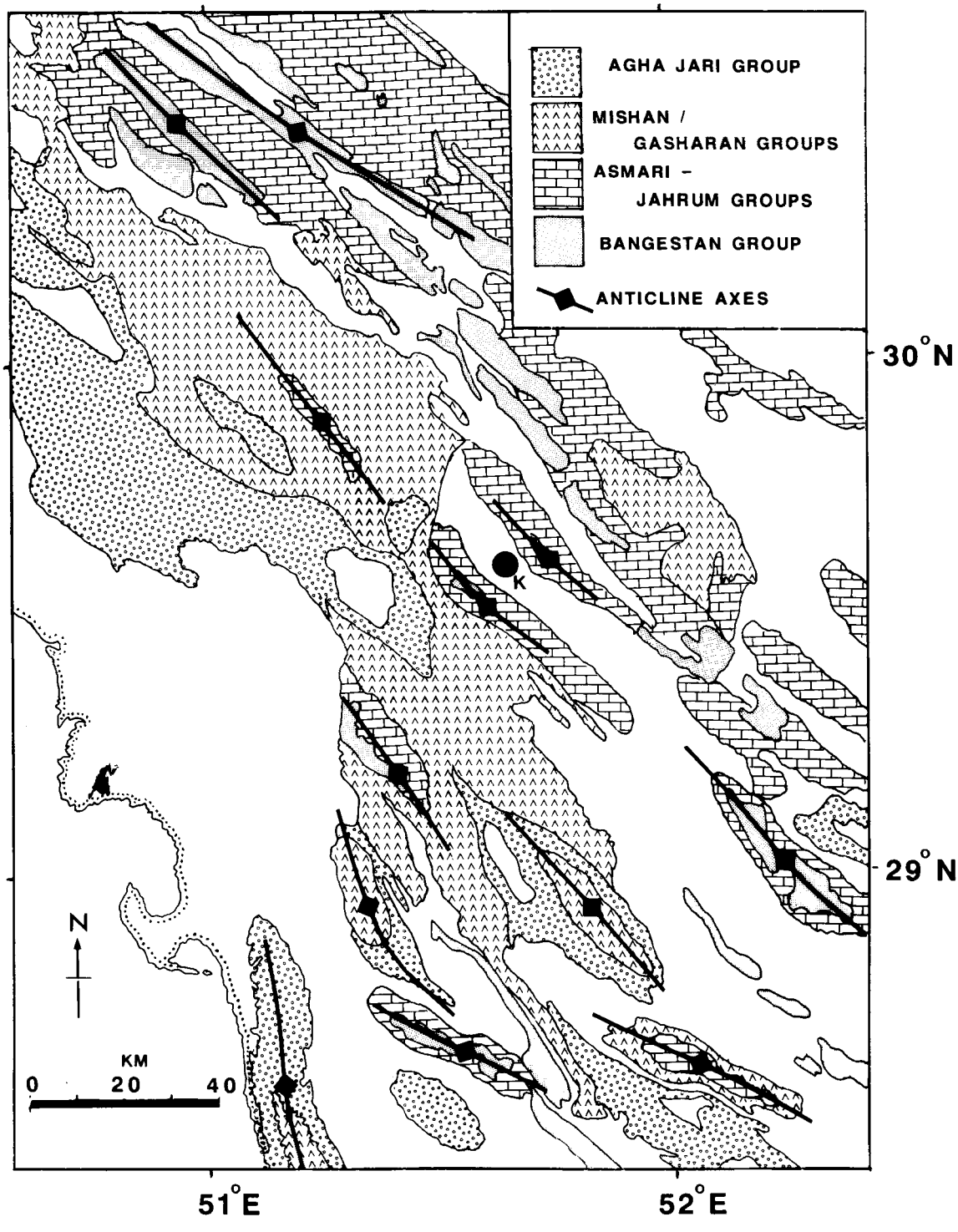

Figure 2. Map showing the main geological features near the town of Kazerun (marked as **K**). The unshaded region corresponds to sediment of Quaternary age. The Agha Jari Formation is of Miocene to Pliocene age and consists primarily of continental conglomerates, sandstone, silt and mud. The Mishan and Gascharan formations are of Miocene age, consisting of limestones, marls and thick evaporites. The Asmari and Jahrum formations consist mainly of limestones of Palaeocene to Oligocene age. The Bangestan group contains limestones and shales of Cretaceous age.

of central Asia, large strike–slip faults cross the range at an oblique angle to the strike. The strike–slip faults there are active today. They are visible at the surface and in satellite images, clearly truncating and offsetting fold axes, and several have moved in strike–slip faulting earthquakes this century (Tapponnier & Molnar 1979; Molnar & Deng 1984; Nelson, McCaffrey & Molnar 1987). Some of the transverse structures in the Tien Shan cross the entire range, and are clearly basement features. The Lesser Himalaya also contains a number of strike–slip faults oblique to the strike of the belt (Valdiya 1976). These trend NNE and NNW, with a trend similar to the subsurface ridges and faults seen

in the adjacent Indian shield. This similarity suggests that the transverse faults are related to the structural features of the underthrusting Indian Shield (Ni & Barazangi 1984). The seismically active fold-and-thrust belt of NW Greece and Albania contains structures that are similar to the Kazerun Line; they appear as transverse valleys almost perpendicular to regional strike, across which fold axes are not continuous. These have been interpreted as strike–slip faults (I.F.P. 1966), but have had no recent large earthquakes associated with them.

This study was motivated by the occurrence of seven moderate-sized (m_b 5.1–5.7) earthquakes in 1986–90 that occurred on or very near the Kazerun Line in the Zagros. Prior to these earthquakes, there had been almost no seismicity on the Kazerun Line that could be studied by teleseismic methods. In this paper we obtain the source parameters of these and other nearby earthquakes. This information will allow us to address the following questions: (1) is the Kazerun Line the surface expression of basement faulting? (2) Is it associated with right-lateral strike–slip faulting, and therefore different from the high-angle reverse faulting nearby? (3) If so, is the direction of slip on the Kazerun Line different from that of the nearby reverse faults? The answers to these questions will help establish the nature of this transverse feature, and its role in the accommodation of shortening between Arabia and Iran. In particular, the slip vectors near the Kazerun Line should indicate whether it behaves as a transform feature (in which slip vector is preserved), or as a structure that requires movement of material parallel to the strike of the belt, thus modifying earlier views that the deformation of the Zagros is 2-D. An understanding of the Kazerun Line may help in the interpretation of similar structures in other fold belts that are either inactive, or have had no recent seismicity that reveals their nature.

2 GEOLOGY AND SEISMICITY OF THE ZAGROS MOUNTAINS

The Zagros mountains contain a thick, almost continuous, sequence of shelf sediments from Palaeozoic to Late Tertiary age, deposited over the infra-Cambrian Hormuz Salt Formation, which itself may be a km or more thick (e.g. Ala 1974; Berberian & King 1981). This sequence is distinct from the rocks of central Iran, and is separated from them by a structure called the Zagros Thrust Line (Fig. 1 also known as Main Zagros Reverse Fault) that marks the NE boundary of the Zagros (Stöcklin 1968). In the Late Cretaceous, ophiolitic-like rocks were emplaced along the NE margin of the Zagros, indicating that some shortening occurred then (Stoneley 1976). However, most of the width of the Zagros is occupied by what is known as the 'Simple Folded Belt' which contains the thick Palaeozoic–Mesozoic–Tertiary shelf deposits that were warped into elongate, open folds in the Miocene onwards (Falcon 1969). There is substantial evidence, summarized by Stöcklin (1968, 1974), Stoneley (1976), Koop & Stoneley (1982) among others, that what is now the Simple Folded Belt of the Zagros was a subsiding passive continental margin on the NE edge of the Arabian shield in the Mesozoic and Tertiary. The sedimentary sequence contains thick evaporite horizons of infra-Cambrian, Jurassic and Tertiary age that are known to decouple structures above and below them, and make it unlikely that there is any direct correlation between the structures in the basement and those at the surface (Lees 1952; Falcon 1969). The basement iself is not exposed, and is known only from exotic blocks of metamorphic rocks brought to the surface in salt plugs (Haynes & McQuillan 1974). The total thickness of sediments above this basement is not known precisely: it is estimated to be around 8–10 km, but might reach greater thicknesses locally, such as in the Dezful embayment near 32°N 49°E (see Morris 1977; Jackson & Fitch 1981).

The Kazerun Line itself is the most prominent of a number of north–south lineations that cross the Simple Folded Belt (Plate 1; Figs 1 and 2). It runs north from the Persian Gulf for about 250 km at longitude 51.5°E. A similar feature occurs near Qir, 200 km SE of Kazerun (Fig. 1). Most of these transverse features do not outcrop as discrete strike–slip faults at the surface, though they are sometimes associated with a deflection of nearby structures into the valleys that suggests a right-lateral component of motion on them (e.g. McQuillan 1973). Such deflection can be clearly seen on a *Landsat 4* image of the Kazerun Line (Plate 1). Falcon (1969) suggests that the Arabian shield (of which the Zagros basement is thought to be a part) is divided into a number of blocks by basement faults of this north–south trend.

Earthquakes occur throughout the 200–300 km width of the Zagros mountains, with an abrupt cut-off in the NE, along the Zagros Thrust Line (Fig. 1). However, except in the NW of the belt, most of the larger ($m_b \geq 5.0$) earthquakes in the Zagros occur along its SW front, between the coast of the Persian Gulf and the 1500 m topographic contour (Jackson & McKenzie 1984; Ni & Barazangi 1986). Except for smaller earthquakes, the highest elevations of the Zagros, which reach 3000–4000 m, are relatively aseismic. Most of the larger earthquakes have fault plane solutions that show high-angle (30–60° dip) reverse faulting on planes parallel to the local strike of the belt (see McKenzie 1972; Jackson & McKenzie 1984). These fault plane solutions are based primarily on *P*-wave first-motion polarities, and their strikes are thus constrained mostly by polarities at regional stations. In this study we use teleseismic *P* and *SH* waveforms to obtain source parameters. *SH* waveforms are particularly useful for constraining the strike of high-angle reverse-fault mechanisms. Only two fault plane solutions are so far available for earthquakes near the Kazerun Line. The first occurred on 1968 June 23 and had first motion polarities at regional stations that suggested a different source orientation from the majority of Zagros earthquakes. The solution published for this event by Jackson & Fitch (1981) involved reverse faulting on a strike parallel to the Kazerun Line. The second event occurred on 1971 April 6. First motion readings published by Jackson & McKenzie (1984) allowed either a thrust or strike–slip solution. We will re-examine both events using *P* and *SH* waveforms.

Various people have studied the depths of the larger Zagros earthquakes using teleseismic *P* waveforms (e.g. Jackson & Fitch 1981; Kadinsky-Cade & Barazangi 1982; Ni & Barazangi 1986). The hypocentres are mostly in the range 8–14 km. These depths are obtained from long-period waveforms of the World Wide Standard Seismograph

Network (WWSSN) and are thus centroid depths: they represent the finite earthquake source by a point, which is the weighted centre of moment release. Since the earthquakes are of magnitude (M_s) ~ 6.0, they will have involved motion on faults of around 10 km dimension. It is therefore safe to assume that the faulting extended to greater depths than the hypocentres and almost certainly into what can be regarded as 'basement' beneath the Hormuz Salt Formation. These studies therefore conclude that the larger earthquakes probably occur on faults in the uppermost basement beneath the sedimentary cover. Such basement faults would be unlikely to propagate to the surface through the several thick evaporite horizons within the sedimentary cover, and this is usually taken as the explanation for the remarkable lack of surface faulting following Zagros earthquakes even as large as M_w 6.7 (e.g. Berberian 1976a, 1977; Berberian & Papastamatiou 1978; Jackson & Fitch 1981; Ambraseys & Melville 1982).

The occurrence of widespread high-angle reverse faulting within the basement led Jackson (1980) to suggest that reverse motion was occurring on reactivated old normal faults that were responsible for the extension and subsidence of the continental margin in the Mesozoic. Such reactivation has since been demonstrated elsewhere (e.g. Stoneley 1982; Badley, Price & Backshall 1989; Roberts 1989; Letouzey 1990), but in the Zagros remains just a plausible speculation and cannot be proved.

In this paper we will use long-period teleseismic *P* and *SH* waveforms to determine the source parameters of nine earthquakes that occurred on or near the Kazerun Line. We will also consider the centroid-moment tensor (CMT) solutions published by Harvard for four events where the data were insufficient for us to model using our technique.

3 DETERMINATION OF SOURCE PARAMETERS

We used first motion polarities and *P* and *SH* waveforms to constrain the earthquake source parameters. First motions were taken from long-period vertical instruments of the WWSSN, and the onset times of these first motions were checked, when possible, with the arrival times recorded on the short-period instrument. When the long-period instrument was unavailable, we read the polarity on short-period instruments only when the onset was recognizable as the instrument response to a delta function, and at an arrival time with a small traveltime residual (see Jackson & McKenzie 1984). We did not read first-motion polarities from the narrow-band instruments of the SRO or ASRO networks, which have too emergent a response for this purpose. The first motions for the events we studied here are shown in Fig. 3.

For *P* and *SH* waveform analysis we used McCaffrey & Abers's (1988) version of Nábĕlek's (1984) inversion procedure, which minimizes, in a least-squares sense, the misfit between observed and synthetic seismograms. This procedure is now too routine to justify detailed description. The reader is referred to MCCaffrey & Náblělek (1987), Nelson *et al.* (1987), Fredrich, McCaffrey & Denham (1988) for details. The procedure assumes that the source can be represented as a point (the centroid) in space, but not in time. The time history of displacement on the fault is represented by a source-time function made up of a series of overlapping isosceles triangles. The seismograms are formed by the addition of direct *P* or *SH* waves with the surface reflections *pP*, *sP* and *sS* and near-source multiples. Amplitudes are corrected for geometrical spreading, and for anelastic attenuation using a Futterman (1962) *Q* operator with a value for t^* of 1.0 s for P and 4.0 s for *SH* waves. Uncertainties in t^* lead to uncertainties in source duration and seismic moment, but have only a small effect on centroid depth and source orientation. To avoid upper mantle triplications and interference from core phases, *P* waveforms are used in the distance range 30–90°, and *SH* waves in the range 30–75°.

The inversion procedure adjusts the relative amplitudes of the source-time function elements, the centroid depth, the seismic moment, and the source orientation (strike, dip, rake) to minimize the misfit between observed and synthetic seismograms. We refer to this solution as the 'minimum misfit solution'. The covariance matrix associated with this solution usually underestimates, sometimes seriously, the true uncertainities associated with the source parameters (see McCaffrey & Nábělek 1987). A better estimate of the real errors is found by fixing some of the source parameters at values close to but different from those of the minimum misfit solution, and seeing whether the match of observed-to-synthetic seismograms deteriorates (see McCaffrey & Nábělek 1987; Nelson, McCaffrey & Molnar 1987; Fredrich *et al.* 1988; Molnar & Lyon-Caen 1989). We use this procedure to estimate errors here.

Uncertainties in seismic moment and centroid depth arise from errors in the source velocity model. Realistic velocity models are not known in the Zagros. We therefore tried various different models, within a range that we considered likely, to examine their influence on these parameters. In general, we used a velocity model with an average *P* velocity of 6.0 km s^{-1} above the source and 6.8 km s^{-1} below the source. In the next section we will discuss one earthquake in detail to illustrate the procedures we adopted. The other earthquakes are discussed more briefly in the Appendix.

Hypocentral parameters of the earthquakes we studied are listed in Table 1. Their epicentres are plotted in Fig. 1, and are likely to be in error by up to 15 km (Ambraseys 1978; Berberian 1979).

4 THE EARTHQUAKE OF 1988 DECEMBER 6

This earthquake, of m_b 5.5, is typical of the group of events that occurred near the Kazerun Line between 1986 and 1990 (Fig. 1 and Table 1) in that *P* amplitudes were small, and in particular, much smaller than *SH* amplitudes. Very few first motions were large enough to be read on long-period WWSSN instruments, and first motions alone are unable to constrain the fault-plane solution effectively (Fig. 3): the few compressional polarities that are available are consistent with both right-lateral strike–slip faulting on a north–south fault and with high-angle reverse faulting striking NW–SE.

Observed waveforms for this earthquake are shown in Fig. 4. *SH* waveforms are well distributed in azimuth and are of large amplitude. *P* amplitudes are at least a factor of 3 smaller. The minimum misfit solution returned by the inversion procedure is a strike–slip mechanism, consistent

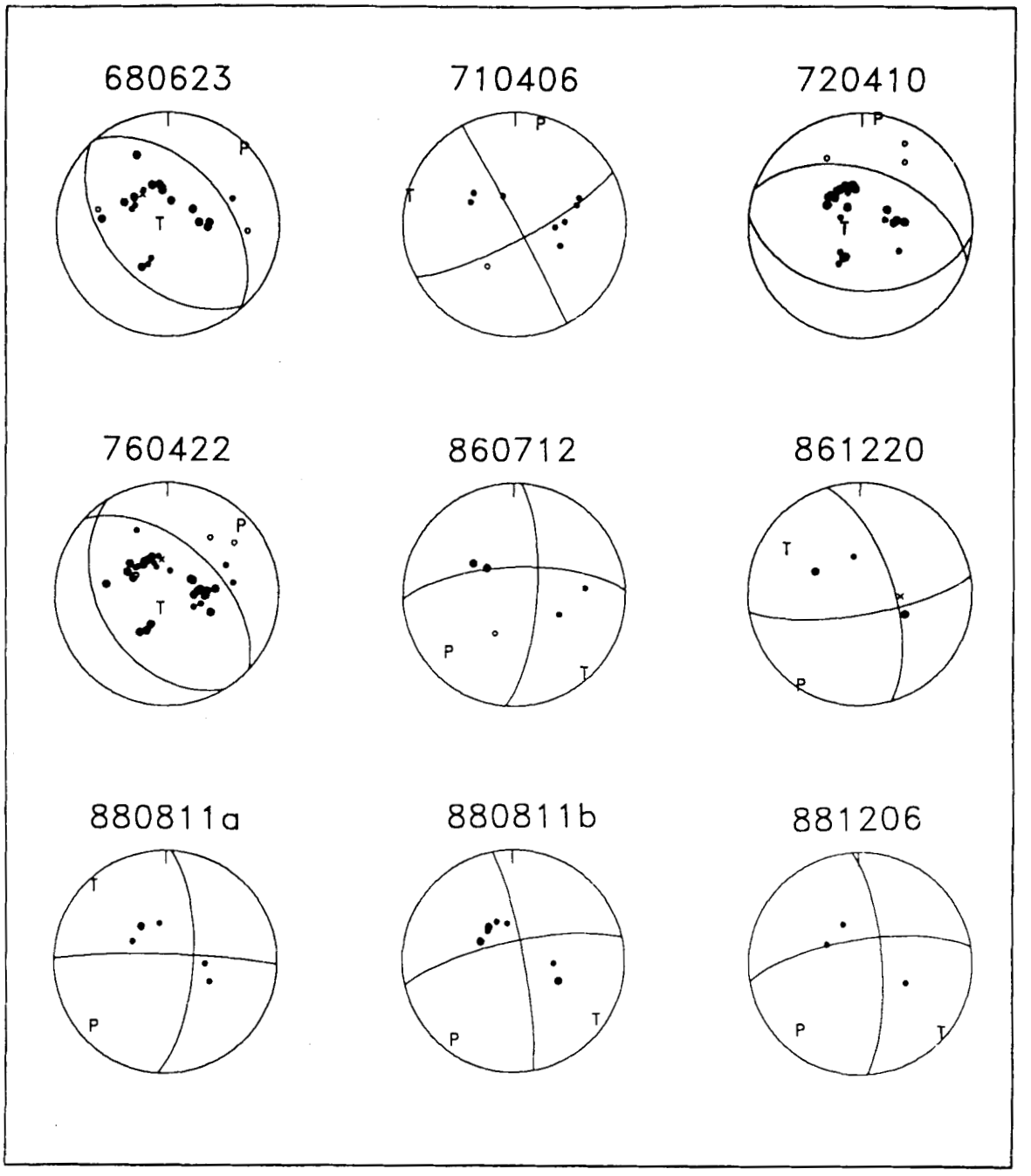

Figure 3. Lower hemisphere equal-area projections of *P*-wave first-motion data. Station positions have been plotted using a velocity of 6.8 km s^{-1}, as used in the waveform synthesis. In each case the nodal planes are those of the minimum misfit solution obtained from waveform inversion. Filled circles are compressional first motions and open circles are dilatations. Large symbols are readings taken from WWSSN long period records. Nodal onsets are marked as crosses. *P* and *T* axes are marked by letters. The earthquake date (year, month, day) is above each focal sphere.

with right-lateral faulting on a north–south fault. At first glance, it would appear that the main constraint on this solution is provided by the large and abundant *SH* waveforms, rather than the *P* waveforms. The observed *SH* waveforms are obviously well matched by the minimum misfit solution. However, the *SH* radiation pattern, whose nodal planes are arranged in cross oriented NE–SW and NW–SE, is consistent with either north–south right-lateral strike–slip faulting (as in Fig. 4) or with high-angle reverse faulting striking NW–SE. Both mechanisms are also allowed by first-motion polarities (Fig. 3), and these are the two possibilities that are most likely and which we wish to distinguish. (Recall that previous authors had inferred a north–south right-lateral strike–slip nature to the Kazerun Line, and that most of the existing fault plane solutions in the Zagros show reverse faulting with a NW–SE strike.) We must therefore address whether the waveform data are able to distinguish these two mechanisms.

Table 1. List of earthquakes studied in this paper. Locations and origin times are taken from ISC listings prior to 1988. After this PDE locations are used. The event letters correspond to those used in the text.

Event	Year	Month	Day	Origin Time	Lat.	Long.	m_b
A	1968	06	23	09:16:18.6	29.81	51.16	5.2
B	1971	04	06	06:49:52.9	29.80	51.88	5.2
C	1972	04	10	02:06:53.2	28.43	52.82	6.1
D	1976	04	22	17:03:07.9	28.71	52.12	6.0
†E	1981	04	01	10:16:59.2	29.84	51.50	5.4
F	1986	07	12	07:54:26.8	29.96	51.58	5.7
G	1986	12	20	23:47:08.9	29.98	51.62	5.5
H	1988	08	11	16:00:07.5	29.97	51.57	5.3
I	1988	08	11	16:04:45.6	29.97	51.67	5.7
†J	1988	08	30	17:30:21.3	29.95	51.70	4.9
K	1988	12	06	13:20:41.0	29.94	51.65	5.5
†L	1989	05	03	09:13:20.0	29.96	51.65	5.1
†M	1990	12	16	22:18:50.0	29.05	51.31	5.3

'†' Events for which insufficient waveforms were available to model. Here the Harvard CMT solution is used.

In Fig. 5 we compare selected *P* and *SH* waveforms of our minimum misfit solution (top line), with those for an inversion (bottom line) in which the fault orientation was that of a reverse-fault striking NW–SE with an *SH* radiation pattern similar to that of the minimum misfit solution. To obtain the solution in line C we computed the thrust solution with the same *SH* radiation pattern as the strike–slip fault in line A and used this as the starting point for the inversion. We then allowed all parameters to vary in the inversion. Unlike the minimum misfit solution in the top line, the solution in the bottom line is unable to fit the amplitudes of both the *P* and *SH* waveforms simultaneously. The *P* amplitudes predicted by the reverse-fault mechanism are much too large relative to the *SH* amplitudes. The reason for this is clear: in the strike–slip solution (top line) the station positions on the focal sphere are all close to the nodal planes of the *P*-radiation pattern, and are

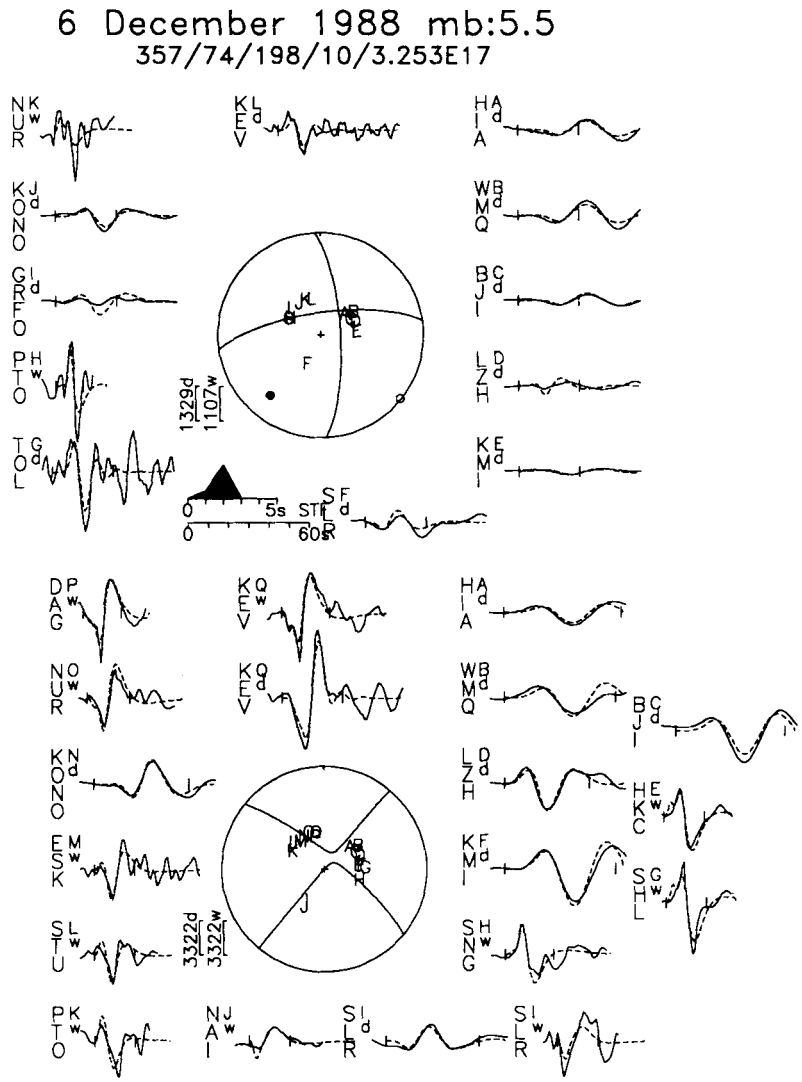

Figure 4. The *P* and *SH* waveforms for the minimum-misfit solution obtained for the event of 1988 December 6 (Event J). The values beneath the event header give the strike, dip, rake, depth and seismic moment (in units of Nm). The upper sphere shows the *P*-wave radiation pattern and the lower sphere that for *SH*. Both are lower hemisphere projections. The station code by each waveform is accompanied by a letter corresponding to its position within the focal sphere. These are ordered clockwise by azimuth. A 'w' corresponds to WWSSN data and a 'd' to data from the GDSN network. The solid lines are the observed waveforms, the dashed lines are the synthetic waveforms. The inversion window is marked by solid bars at either end of the waveform. *P* and *T* axes within the sphere are represented by solid and open circles respectively. The source-time function is shown below the *P* focal sphere, with the waveform time scale below this. Waveform amplitude scales are to the left of the focal sphere.

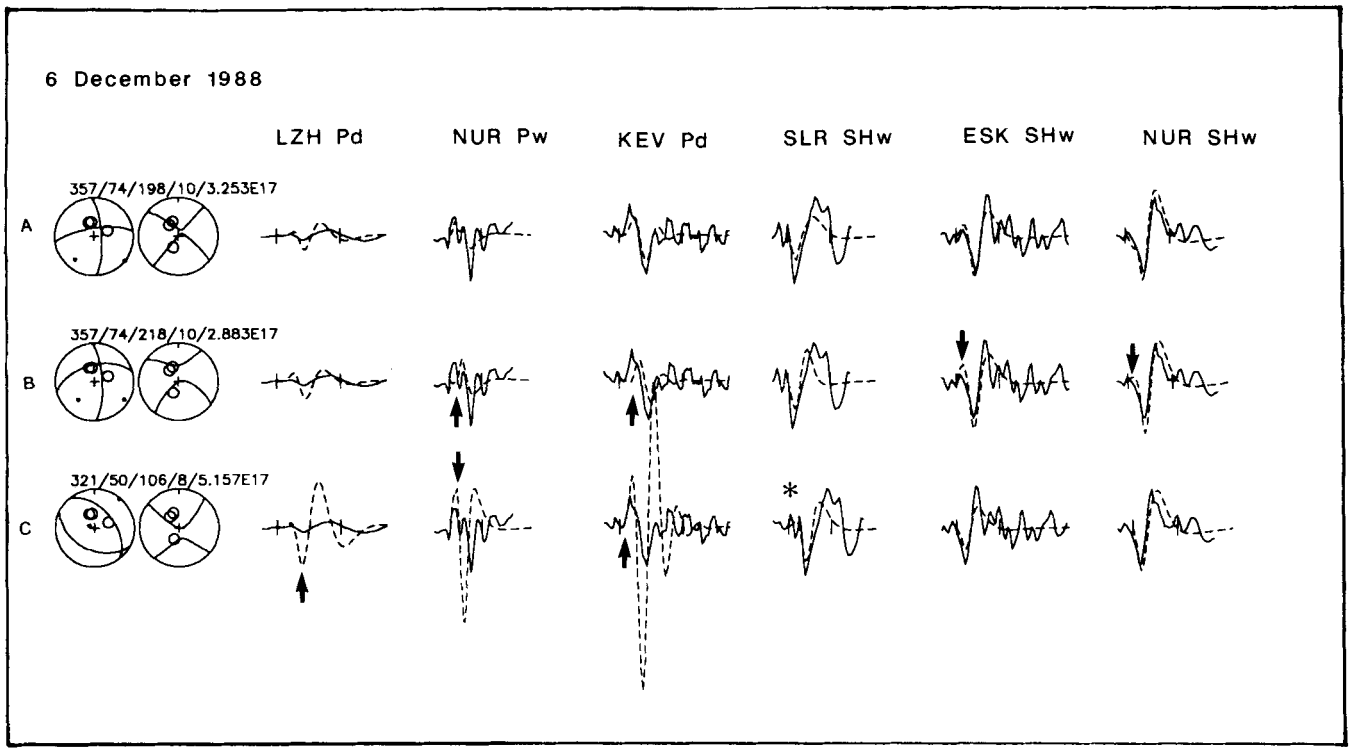

Figure 5. Comparison of possible fault-plane solutions for the event of 1988 December 6. Waveforms are shown at six representative stations. In line A, synthetic waveforms are from the minimum misfit solutions. Line B shows synthetic waveforms for the orientation given by the Harvard moment tensor solution. Line C shows a thrust solution which gives a satisfactory fit to first-motion readings and which is characteristic of thrust events seen in the Zagros. In this, and in subsequent similar diagrams, an arrow signifies a poorer fit than the minimum misfit solution and an '*' an improvement in fit.

consequently of small amplitude. For the reverse-fault solution, these stations are in the middle of the compressional *P* quadrant, and have much larger amplitude. In other words, the smallness of the *P* waveforms is in itself important information, which is consistent with the strike–slip but not with the reverse fault solution.

A centroid-moment tensor (CMT) solution, obtained by Harvard University, was also published for this event in the Preliminary Determination of Epicentres (PDE) issued by the USGS. The orientation of the CMT solution differs only by 20° in rake from that of our minimum misfit solution. In the middle line of Fig. 5 we show the waveforms for an inversion in which the strike, dip and rake were held at the values given by the CMT solution, and only the source time function, centroid depth and moment were allowed to be free. The synthetic waveforms in the top and middle lines are a little different; the fit to some of the observed seismograms at stations marked by arrows in the middle row is perhaps marginally worse than in the top row. This procedure illustrates how we estimate uncertainties in source orientation. For example, to examine rake, we would fix the rake at a value different from that of the minimum misfit solution and allow all other parameters to be free in the inversion. If the resultant fit of observed and synthetic seismograms was significantly poorer than the fit for the minimum misfit solution, we would conclude that the value of rake chosen was outside the acceptable range. In this way we estimated the uncertainties for this earthquake to be ±10° in strike, −10/+5° in dip, ±15° in rake, and ±2 km in depth.

We also investigated the effect of a likely range of source velocity models on the inversion. Fig. 6 shows selected waveforms at a number of stations for inversions carried out in the different velocity models listed in Table 2. The fit of synthetic and observed waveforms is barely different in each case. The source orientations are only a few degrees different from that of the minimum misfit solution (row D): differences that are anyway less than the uncertainty we estimated for each of these parameters. The main effect of changing velocity structure is to change centroid depth, by

Table 2. Velocity structures used in Fig. 6.

Line	Layer	Depth	V_p	V_s	ρ
A	half space		6.5	3.5	2.7
B	half space		6.7	3.75	2.8
C	1	7	5.7	3.4	2.6
	half space		6.8	3.9	2.9
D	1	7	6.0	3.7	2.75
	half space		6.8	3.9	2.9

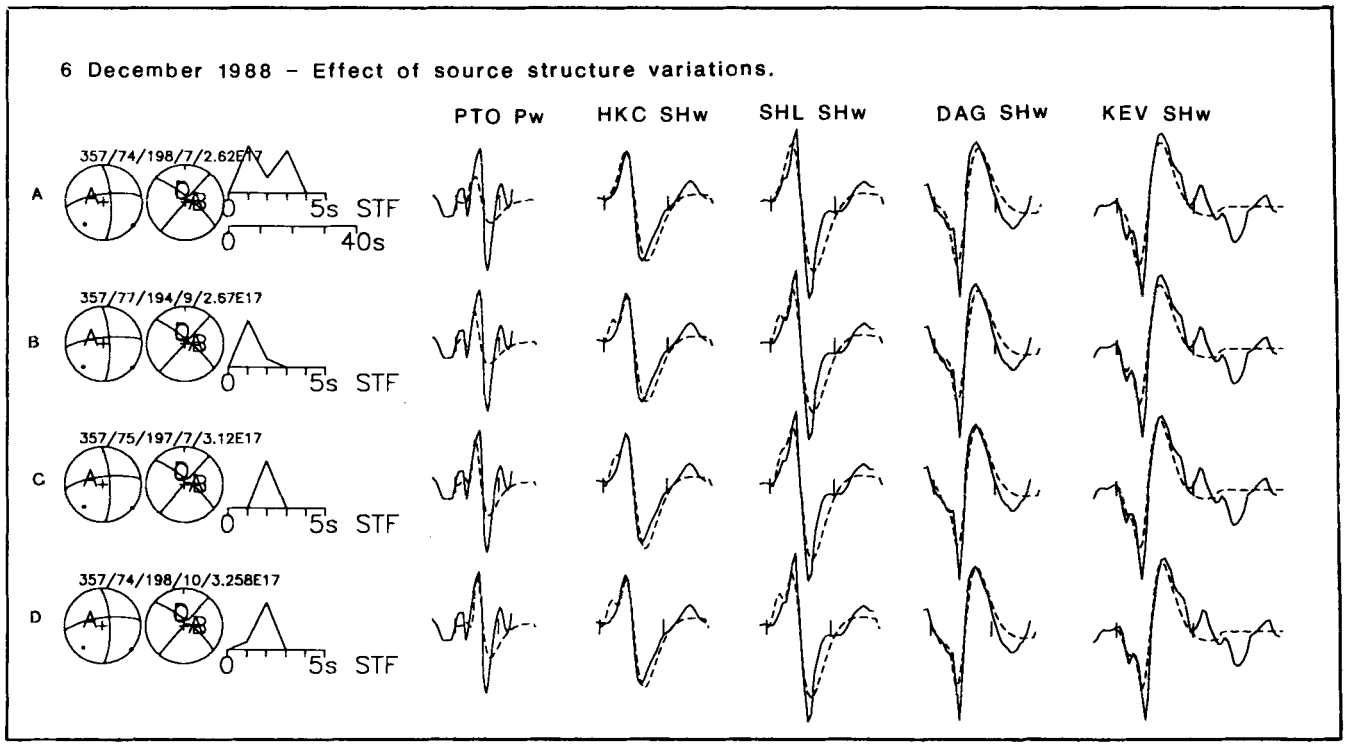

Figure 6. Tests showing the influence of source velocity structure on the minimum-misfit solution for the event of 1988 December 6. The velocity structure used in each line is given in Table 2. Each line shows the *P* and *SH* radiation patterns, the source-time function and the resulting waveform fits for 5 stations. Line D shows the structure which was used to obtain the minimum misfit solution in Fig. 4.

up to 3 km in this case, and seismic moment, by up to 20 per cent. Small changes are also observed in the source time function. Thus we are confident that reasonable changes to the source velocity structure will not affect our estimate of the source orientation (the principal interest of this paper) to a greater extent than the errors we would anyway estimate from our other tests.

We investigated eight other earthquakes in the manner outlined for this event. Each one is discussed in the Appendix. In particular, the observation that the *P* waveforms were much smaller in amplitude than the *SH* waveforms (as discussed in Fig. 4) was an important indication that several of the earthquakes had strike–slip mechanisms.

5 RESULTS

From an analysis of long period *P* and *SH* body waves we were able to estimate source parameters, and their uncertainties, for nine earthquakes in the vicinity of the Kazerun Line. The fault plane solutions for these earthquakes are shown in Fig. 7. We also include in Fig. 7 the fault-plane solutions for four additional earthquakes, for which Harvard CMT solutions are available, but whose body waves were too small for us to analyse by the technique illustrated above. The source parameters for these earthquakes are listed in Table 3.

6 DISCUSSION

Of the nine earthquakes whose body waveforms we analysed, the five whose epicentres lie close to the Kazerun

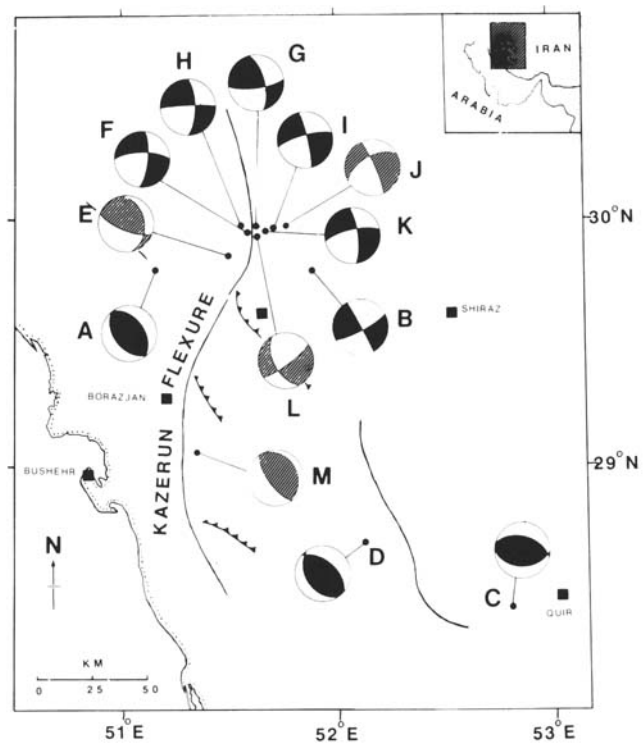

Figure 7. Summary map of the minimum misfit solutions for events studied in this paper. Fault plane solutions are shown as lower hemisphere projections joined to their epicentral locations. The letter beside each focal sphere identifies each event in Tables 1 and 3. The focal spheres with the striped shading (E and K) are Harvard CMT solutions.

Table 3. Minimum misfit solution and errors for events modelled in this study. The strike, dip and rake for events *F, G, H, I, K* are given for the nodal planes that we think are the fault planes. '†' indicates a Harvard CMT solution. The reported depths for these four events are fixed values so we indicate them with a '*'.

Event	Date	M_w	Solution					Errors			
			Strike (°)	Dip (°)	Rake (°)	Depth (km)	M_o $\times 10^{16}$ (Nm)	Strike (°)	Dip (°)	Rake (°)	Depth (km)
A	23.6.68	5.5	136	45	88	9	22	-15/+10	-4/+5	-10/+15	±3
B	6.4.71	5.3	62	79	2	6	7.2	±25	-12/+10	-15/+20	-2/+6
C	10.4.72	6.6	288	49	99	9	844	±20	-8/+10	-15/+20	±3
	multiple	(6.7)	322	40	98	10	369				
D	22.4.76	5.7	312	52	80	7	38	-15/+10	-7/+10	±15	±3
†E	1.4.81	5.4	351	34	144	15*	7.8				
F	12.7.86	5.5	004	73	-159	4	26	-8/+10	±15	-15/+20	-2/+4
G	20.12.86	5.3	344	65	163	8	11	±10	-17/+10	-30/+10	±3
H	11.8.88a	5.5	003	69	-175	7	24	-18/+10	-15/+5	-18/+10	-4/+3
I	11.8.88b	5.8	350	82	-166	9	65	-16/+10	-10/+9	-12/+9	-3/+2
†J	30.8.88	5.1	337	83	-147	15*	6.1				
K	6.12.88	5.6	357	74	198	10	32	±10	-10/+5	±15	±2
†L	3.5.89	5.1	153	55	-166	15*	8.4				
†M	16.12.90	5.7	144	67	87	15*	41				

Line (events *F, G, H, I, K*) all have strike–slip mechanisms (Fig. 7) and lie within a small area. The fact that the ISC locations appear to form a line perpendicular to the trend of the Kazerun Line is not significant. The probable errors in the locations of these epicentres are in the region of 15 km (Ambraseys 1978; Berberian 1979), and thus they could all have occurred on the Kazerun Line itself. The Kazerun Line is visible as a north–south striking fault on the surface in the vicinity of these events and although none of these earthquakes were associated with a surface break the fault shows evidence of past right-lateral motion. Each of the fault plane solutions for these five earthquakes contains a nodal plane that is parallel to the Kazerun Line in their epicentral regions, and if these nodal planes were the fault planes, the sense of motion on each would be right-lateral strike–slip. This has always been inferred, from geological evidence, to be the sense of motion associated with the Kazerun Line and other similar structures that cross the Zagros (e.g. Stöcklin 1968; Falcon 1969, McQuillan 1973). Furthermore the known macroseismic areas for these events lie on the line of the fault and are orientated north–south (see Appendix, event F). Such macroseismic locations are likely to be more accurate than the instrumental locations for earthquakes of this size. We therefore conclude that the Kazerun Line and the Kazerun Fault trace represent the surface expression of a buried right-lateral strike–slip fault with a north–south strike (the average strike of the north–south nodal planes in events *F, G, H, I, K* is $356 \pm 9°$).

Our modelling suggests that event B (1971 April 6) also has a strike–slip solution. This is discussed further in the appendix. The ISC location for this event was around 30 km south-east of the cluster of strike–slip events at the northern end of the Kazerun Line and about 50 km NW of the northern end of the Karehbas Fault, a NW striking transverse feature with no earthquakes in recent times. Using a master event technique (Jackson & Fitch 1979) we relocated this event relative to one of those occurring in this cluster. We used 1988 December 6 (event K) as the master as this had the largest number of reporting stations in the ISC bulletin for the events studied. The result indicated that event B really was about 25 km SE of the main cluster of events on the Kazerun Line.

The centroid depths of the five earthquakes on the Kazerun Line vary from 4 to 10 km with typical uncertainties of ±3 km. These depths are those of the conceptual point sources that represent the weighted average position of seismic moment release. To a first approximation we can think of them as points in the centre of the fault planes that moved in each earthquake. These earthquakes were not large, the biggest being only M_w 5.8. We can estimate the approximate size of the fault planes in the following way. The seismic moment, M_0, is given by $M_0 = \mu A \bar{u}$, where μ is the rigidity ($\sim 3 \times 10^{10}\,\mathrm{Nm}^{-2}$), A is the fault area, and $\bar{u}$ is the average displacement. Let us assume that the fault is roughly circular in area with diameter L, and that the ratio $\bar{u}/L$ *is* $\sim 5 \times 10^{-5}$ (see e.g. Scholz, Aviles & Wessnousky 1986). For a seismic moment of 5×10^{17} Nm (Table 3), we would then calculate L to be 8 km. In other words, since the faults are subvertical, rupture in earthquakes of this size would extend about 4 km beneath the centroid depth. The depth to the basement in this area, by which we mean the crystalline metamorphic rocks beneath the overlying sedimentary cover, is not well known. Morris (1977) estimates the depth to magnetic 'basement', based on aeromagnetic surveys, to be about 8 km. We believe it likely that these earthquakes on the Kazerun Line involved faulting in the basement for two reasons: (1) the centroid depths and source dimensions of the earthquakes make faulting at basement depths probable

(to the extent that basement depths are known), and (2) we do not believe that faults with dimensions of 8 km can be contained within a sedimentary column of comparable thickness that contains at least three separate and thick evaporite sequences (at infra-Cambrian, Jurassic and Miocene levels) without involving surface rupture. In other words, if the faults are required to cut through the evaporite horizons to achieve the area necessary for their seismic moment, why do they not also cut through to the surface, as earthquakes of similar size do elsewhere in Iran (see e.g. Ambraseys & Melville 1982)? We think it more probable that the earthquake faulting is predominantly beneath the Hormuz Salt, whose ductility prevents rupture reaching the surface. The Kazerun Line then represents the surface distortion of the folded, deformed sedimentary cover that is decoupled from the motions in the basement.

What is then the significance of the Kazerun Line in the deformation of the Zagros, which must accommodate the convergence between Arabia and central Iran? In Fig. 8 we show the horizontal projections of the slip vectors for the earthquakes in Fig. 7. For the strike–slip earthquakes we studied on the Kazerun Line (*F, G, H, I, K*) and for events *J* and *L*, for which there is only a Harvard CMT solution, we chose the north–south nodal planes as the fault planes.

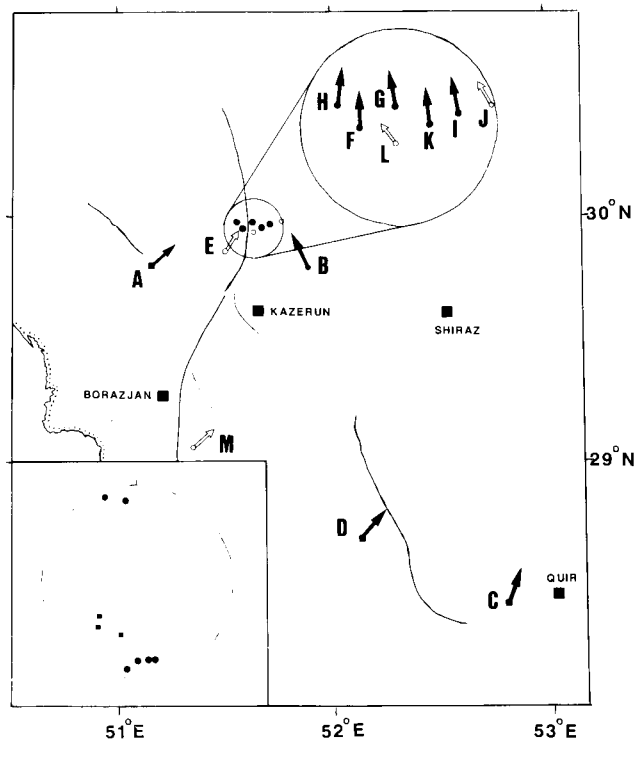

Figure 8. Map showing the horizontal projections of the slip vectors for the earthquakes discussed in this study. These are plotted so as to show motion of the south or west side relative to the north or east. Letters identify the events in Tables 1 and 3. Large filled circles are strike–slip events studied in this paper. Open circles are Harvard CMT solutions. Filled squares are reverse-faulting events studied in this paper. The inset in the bottom left-hand corner shows a stereographic projection of slip vectors for the nine events whose waveforms we studied. Closed circles are strike–slip events, open circles are Harvard CMT solutions and filled squares are reverse faults.

The average slip vector azimuth for events *F, G, H, I, K* is $354 \pm 5°$. If we also consider event *B* in this group then the average slip vector azimuth is 350°. For the three earthquakes we studied that involved high-angle reverse faulting (*A, C, D*), we cannot identify the probable fault plane: however, they are all nearly pure reverse faults, and the two possible slip vectors in each earthquake do not differ by more than 16°. The average azimuth of all six slip vectors for these earthquakes (two per event) is $036 \pm 22°$. The dispersion of the slip vectors in these reverse faulting events is partly related to the curvature of the arc made by the southern Zagros in this region: the anticlines in the NW of Figs 2 and 7 trend ~165°, whereas in the SE, near event *C*, the anticlines trend ~140°. Thus events *A, C* and *D* involved faulting with a strike roughly parallel to the local trend of the anticlines. The two thrusts for which CMT solutions are available (events *E* and *M*) also follow this pattern.

Thus the strike–slip faulting on the Kazerun Line involves slip that is in a different direction from that associated with the reverse faulting and folding. There are two possible explanations for this discrepancy. The first is that the overall motion accommodated by the Kazerun Line is the same as that accommodated by the reverse faults, but that the Kazerun Line rotates about a vertical axis as it moves. This style of deformation is known from elsewhere, such as in Greece (e.g. McKenzie & Jackson 1986; Taymaz, Jackson & McKenzie 1991), but usually involves domains of several rotating subparallel faults. The Kazerun Line seems isolated, and also surrounded by reverse faults (e.g. events *A, E* and *M*). There may be other more subdued transverse structures in the Zagros (Berberian 1976b), but none is as prominent as the Kazerun Line. We do not think this rotational explanation for the slip vector directions on the Kazerun Line is likely. The only other major transverse lineation in the Zagros which appears to be active is the Oman Line. This lies 700 km to the SE at the eastern end of the Zagros fold belt and marks an abrupt change in the pattern of seismicity, separating the fold belt from the Makran subduction zone. It is characterized by thrust faulting and is thought to represent the underthrusting of the Arabian shelf beneath Iran or the indentation of Arabia as a promontory (Kadinsky-Cade & Barazangi 1982).

A second explanation for the discrepant slip direction on the Kazerun Line is that it takes up shortening perpendicular to the strike of the Zagros by a component of extension parallel to the strike of the belt, rather than by crustal thickening. This style of deformation is also known elsewhere, such as in eastern Turkey (e.g. McKenzie 1972) and in central Asia (e.g. Tapponnier & Molnar 1979). In Fig. 9 we show the *P* and *T* axes of the earthquakes in Fig. 7. For the earthquakes we studied, the azimuths of the *P* axes for the reverse faults (three events, average $36 \pm 21°$) and the strike–slip faults (five events, average $36 \pm 7°$) are the same. The average *P*-axis azimuth for all nine earthquakes is $36 \pm 15°$, which is almost perpendicular to the average strike of the anticlines (140–165°). The *T* axes for the strike–slip events are subparallel to the strike of the fold belt. These observations, and the fact that the Kazerun Line appears as a structure on its own rather than as one of a series of parallel faults, suggests to us that this second

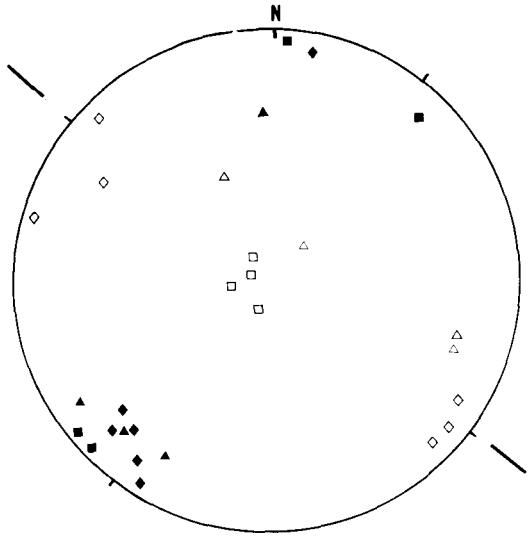

Figure 9. Lower hemisphere projection of the *P* and *T* axes for the events studied in this paper.

explanation is the more likely of the two. The strike–slip motion on the Kazerun Line implies that there is movement of material along strike of the Zagros, and that the deformation in this mountain belt is not strictly 2–D. It is not easy to assess the likely rate of elongation parallel to the strike of the Zagros that is caused by the Kazerun Line and similar structures. It is clear from the anticlines and reverse faulting earthquakes near the Kazerun Line that it does not accommodate all the shortening at its position within the belt. Regional elevations near the Kazerun Line are not noticeably different from those elsewhere in the Simple Folded Belt. These observations, combined with the modest level of recent and historical seismicity (Ambraseys & Melville 1982), suggest to us that the rate of motion on the Kazerun Line is relatively slow.

At the surface the Kazerun Line appears as an oblique interruption to the otherwise regular series of anticline ridges. The earthquakes we have studied demonstrate that this feature is not merely an instability in the folding of the sediments, but is the surface expression of a buried right-lateral strike–slip fault. Could this fault simply be a lateral ramp on one or a series of thrust faults, as envisaged in, for example, the Canadian Rockies or the Appalachians (e.g. Harris 1970; Dahlstrom 1970; Boyer & Elliott 1982)? We do not think the Kazerun Line (or fault) is such a lateral ramp, for two reasons: (1) the slip vectors on the Kazerun Line are different from those of the reverse faults, and (2) the reverse faults that occur in the Zagros have, almost without exception, relatively steep dips in the range 30–60°. Moreover, the reverse faults are active across a considerable width of the range (Jackson & McKenzie 1984). We do not doubt that there is a decoupling between the metamorphic basement and the sedimentary cover above the Hormuz Salt, but if this takes the form of a low-angle thrust, it is evidently aseismic. The high-angle reverse faulting occurs in earthquakes that can be much larger than the strike–slip events we studied on the Kazerun Line (see e.g. event *C* in Table 3), and the same arguments about source dimensions that we made for the strike–slip earthquakes apply equally to the reverse faults: their source dimensions are too big, and their centroid depths are too great for it to be likely that such faults can be contained within the sedimentary cover without producing surface ruptures. In other words, we agree with Jackson (1980), Jackson & Fitch (1981) and Ni & Barazangi (1986) that the reverse faulting earthquakes probably occur within the metamorphic basement.

The Kazerun Line thus appears to be a fundamental structure in the Zagros, confirming previous inferences based on its influence on the sedimentary record. The Kazerun Line is a recognizable feature in the isopach and facies maps of the Zagros since at least the middle Jurassic (e.g. Setudehnia 1978; Koop & Stoneley 1982). It may, as Falcon (1969) implies, be one of a system of much older, inherited structures with a north–south strike within the Arabian shield. Its past sense of motion could therefore have been different from its present day activity, which is that of a right-lateral strike–slip fault oblique to the regional strike, causing some elongation of the Zagros perpendicular to the direction of shortening.

7 CONCLUSIONS

The Kazerun Line is a valley that obliquely crosses the regular trend of anticline axes in the Zagros mountains. At the surface, the anticline axes appear to die out, or bend, as they approach the valley and do not cross it. The earthquakes we have studied demonstrate that the Kazerun Line is the surface expression of a buried right-lateral strike–slip fault. The source dimensions of these earthquakes, and their centroid depths, suggest to us that this buried faulting affects the metamorphic basement and is not confined to within the sedimentary cover. High-angle reverse faulting earthquakes also occur near the Kazerun Line . The reverse faults have slip vectors that are different from those of the strike–slip earthquakes on the Kazerun Line, though both types have similar *P*-axis azimuths. We conclude that the right-lateral strike–slip motion on the Kazerun Line contributes to the shortening between Arabia and central Iran by introducing an elongation of the Zagros parallel to the strike of the belt, though the rate of such elongation is probably small compared with the rate of shortening.

Strike–slip faulting that achieves shortening within mountain belts by along-strike elongation is not particularly rare, and has been known for some time in Asia (e.g. Molnar & Tapponnier 1975; Tapponnier & Molnar 1979). Transverse interruptions to the otherwise regular fold axes in a mountain belt have also been described elsewhere, such as in the Canadian Rockies and the Appalachians (e.g. Harris 1970; Dahlstrom 1970; Boyer & Elliott 1982). The

importance of this study is that it demonstrates that transverse irregularities in belts of folded sediments may be related to basement faulting, and not just to lateral ramps within the thrust sheets that deform the sedimentary cover.

ACKNOWLEDGMENTS

We would like to thank Bernard Dost of the Orfeus Data Center in Utrecht and Jackie Shaw of BGS Global Seismology Unit in Edinburgh for their help and hospitality while collecting data for this work. We thank D. McKenzie, T. Taymaz, A. G. Smith, A. D. Smith, D. McCormack and R. Stoneley for helpful discussions. M. Berberian and M. Barazangi made helpful comments on an earlier version of this paper. CB was supported by the Natural Environment Research Council under grant no. GT4/89/GS/12. This is Cambridge Earth Sciences Contribution No. 3055.

REFERENCES

Ala, M., 1974. Salt diapirism in southern Iran, *Am. Assoc. Petrol. Geol. Bull.*, **58,** 1758–1770.

Ambraseys, N. N., 1978. The relocation of epicentres in Iran, *Geophys. J. R. astr. Soc.*, **53,** 117–121.

Ambraseys, N. N. & Melville, C. P., 1982. *A history of Persian earthquakes,* Cambridge University Press, Cambridge.

Badley, M. E., Price, J. D. & Backshall, L. C., 1989. Inversion, reactivated faults and related structures: seismic examples from the North Sea, in *Inversion Tectonics,* pp. 201–219, eds Cooper, M. A. & Williams, G. D., Spec. Publ. Geol. Soc. Lond., **44**.

Berberian, M., 1976a. Contributions to the seismotectonics of Iran (Part 2), *Rep. geol. Surv. Iran,* **39**.

Berberian, M., 1976b. Generalized fault map of Iran, *Geological Survey of Iran,* 1 Map.

Berberian, M., 1977. Contributions to the seismotectonics of Iran (Part 3), *Rep. geol. Surv. Iran,* **40**.

Berberian, M., 1979. Evaluation of the instrumental and relocated epicentres of Iranian earthquakes, *Geophys. J. R. astr. Soc.*, **58,** 625–630.

Berberian, M. & Papastamatiou, D., 1978. Khurgu (north Bandar Abbas, Iran) earthquake of March 21, 1977: a preliminary field report and seismotectonic discussion, *Bull. seism. Soc. Am.*, **68,** 411–428.

Berberian, M. & King, G., 1981. Towards a paleogeography and tectonic evolution of Iran, *Can. J. Earth Sci.*, **18,** 210–265.

Boyer, S. E. & Elliott, D., 1982. Thrust Systems, *Am. Assoc. Petrol. Geol. Bull.*, **66,** 1196–1230.

Colmann-Sadd, S. P., 1978. Fold development in Zagros Simply Folded Belt, Southwest Iran, *Am. Assoc. Petrol. Geol. Bull.*, **62,** 984–1003.

Dahlstrom, C. D. A., 1970. Structural geology in the eastern margin of the Canadian Rocky Mountains, *Bull. Can. Petrol. Geol.*, **18,** 332–406.

Dewey, J. W. & Grantz, A., 1973. The Ghir Earthquake of April 10, 1972 in the Zagros Mountains of Southern Iran: seismotectonic aspects and some results of a field reconnaissance, *Bull. seism. Soc. Am.*, **63,** 2071–2090.

Dziewonski, A. M. & Woodhouse, J. H., 1983. An experiment in the systematic study of global seismicity: centroid-moment tensor solutions for 201 moderate and large earthquakes of 1981, *J. geophys. Res.*, **88,** 3247–3271.

Dziewonski, A. M., Ekström, G., Franzen, J. E. & Woodhouse, J. H., 1987a. Centroid-moment tensor solutions for July–September 1986, *Phys. Earth planet. Inter.*, **46,** 305–315.

Dziewonski, A. M., Ekström, G., Franzen, J. E. & Woodhouse, J. H., 1987b. Centroid-moment tensor solutions for October–December 1986, *Phys. Earth planet. Inter.*, **48,** 5–17.

Falcon, N. L., 1969. Southern Iran: Zagros Mountains, in *Mesozoic–Cenozoic Orogenic Belts,* ed. Spencer, A., Spec. Publ. geol. Soc. Lond., **4,** 199–211.

Fredrich, J., McCaffrey, R. & Denham, D., 1988. Source Parameters of Seven Large Australian Earthquakes determined by Body Waveform Inversion, *J. geophys. Res.*, **95,** 1–13.

Futterman, W. I., 1962. Dispersive Body Waves, *J. geophys. Res.*, **67,** 5279–5291.

Harris, L. D., 1970. Details of Thin-Skinned Tectonics in Parts of Valley and Ridge and Cumberland Plateau Provinces of Southern Appalachians, in *Studies of Appalachian Geology: Central and Southern,* pp. 161–173, eds Fisher, G. W., Pettijohn, F. J., Reed, J. C. & Weaver, K. N., Wiley Interscience Publishers, New York.

Haynes, S. J. & McQuillan, H., 1974. Evolution of the Zagros Suture Zone, Southern Iran, *Bull. geol. Soc. Am.*, **85,** 739–744.

I. F. P., 1966. *Etude géologique de l'Epire (Grèce nord-occidentale),* (Two volumes), Editions Technip, Paris. (Institute of Geology and Mineral Exploration, Athens & Institut Français du Petrole).

Jackson, J. A., 1980. Reactivation of basement faults and crustal shortening in orogenic belts, *Nature,* **283,** 343–346.

Jackson, J. A. & Fitch, T., 1979. Seismotectonic implications of relocated aftershock sequences in Iran and Turkey, *Geophys. J. R. astr. Soc.*, **57,** 209–229.

Jackson, J. A. & Fitch, T., 1981. Basement faulting and the focal depths of the larger earthquakes in the Zagros mountains (Iran), *Geophys. J. R. astr. Soc.*, **64,** 561–586.

Jackson, J. A. & McKenzie, D. P., 1984. Active tectonics of the Alpine–Himalayan Belt between western Turkey and Pakistan, *Geophys. J. R. astr. Soc.*, **77,** 185–264.

Kadinsky-Cade, K. & Barazangi, M., 1982. Seismotectonics of southern Iran: the Oman Line, *Tectonics,* **1,** 389–412.

Koop, W. J. & Stoneley, R., 1982. Subsidence history of the Middle East Zagros Basin, Permian to Recent, *Phil. Trans. R. Soc. Lond.*, **305,** 149–168.

Lees, G. M., 1952. Foreland folding, *Q. J. geol. Soc. Lond.*, **108,** 4–34.

Letouzey, J., 1990. Fault reactivation, inversion and fold-thrust belt, in *Petroleum and Tectonics in Mobile Belts,* pp. 101–128, eds Letouzey, J., Editions Technip, Paris.

McCaffrey, R. & Nábělek, J., 1987. Earthquakes, gravity, and the origin of the Bali Basin: an example of a nascent continental fold-and-thrust belt, *J. geophys. Res.*, **92,** 441–460.

McCaffrey, R. & Abers, G., 1988. SYN3: A program for inversion of Teleseismic Body Wave Forms on Microcomputers, *Air Force Geophysics Laboratory Technical Report, AFGL-TR-88-0099,* Hanscomb Air Force Base, MA.

McKenzie, D., 1972. Active tectonics of the Mediterranean region, *Geophys. J. R. astr. Soc.*, **30,** 109–185.

McKenzie, D. & Jackson, J., 1986. A block model of distributed deformation by faulting, *J. geol. Soc. Lond.*, **143,** 249–253.

McQuillan, H., 1973. A geological note on the Qir earthquake, SW Iran, April 1972, *Geol. Mag.*, **110,** 243–248.

Molnar, P. & Tapponnier, P., 1975. Cenozoic tectonics of Asia: effects of a continental collision, *Science,* **189,** 419–426.

Molnar, P. & Deng, Q. 1984. Faulting associated with large earthquakes and the average rate of deformation in central and eastern Asia, *J. geophys. Res.*, **89,** 6203–7227.

Molnar, P. & Lyon-Caen, H. 1989. Fault plane solutions of earthquakes and active tectonics of the Tibetan Plateau and its margin, *Geophys. J. Int.*, **99,** 123–153.

Morris, P., 1977. Basement structure as suggested by aeromagnetic surveys in S.W. Iran, *Oil Service Company of Iran,* internal report.

Nábělek, J., 1984. Determination of Earthquake source Parameters from Inversion of Body Waves, *PhD thesis*, M.I.T.

Nelson, M. R., McCaffrey, R. & Molnar, P., 1987. Source parameters for 11 earthquakes in the Tien Shan, central Asia, determined by *P* and *SH* waveform inversion, *J. geophys. Res.*, **92,** 12 628–12 648.

Ni, J. & Barazangi, M., 1984. Seismotectonics of the Himalayan Collision Zone: geometry of the underthrusting Indian Plate beneath the Himalaya, *J. geophys. Res.*, **89,** 1147–1163.

Ni, J. & Barazangi, M., 1986. Seismotectonics of the Zagros continental collision zone and a comparison with the Himalayas, *J. geophys. Res.*, **83,** 8205–8218.

Roberts, D. G., 1989. Basin inversion in and around the British Isles, in *Inversion Tectonics*, pp. 131–150, eds Cooper, M. A. & Williams, G. D., Spec. Publ. Geol. Soc. Lond., **44**.

Scholz, C. H., Aviles, C. A. & Wessnousky, S. G., 1986. Scaling differences between large interplate and intraplate earthquakes, *Bull. seism. Soc. Am.*, **76,** 65–70.

Sengor, A. M. C. & Kidd, W., 1979. Post-collisional tectonics of the Turkish–Iranian Plateau and a comparison with Tibet, *Tectonophysics*, **55,** 361–379.

Setudehnia, A. 1978. The Mesozoic sequence in South-East Iran and adjacent areas, *J. Petrol. Geol.*, **1,** 3–42.

Stöcklin, J., 1968. Structural history and tectonics of Iran: a review, *Am. Assoc. Petrol. Geol. Bull.*, **52,** 1229–1258.

Stöcklin, J., 1974. Possible ancient continental margins in Iran, in *The geology of continental margins*, pp. 873–887, eds Burk, C. A. & Drake, C. L., Springer, New York.

Stoneley, R., 1976. On the origin of ophiolite complexes in the southern Tethys region, *Tectonophysics*, **25,** 303–322.

Stoneley, R., 1982. On the structural development of the Wessex basin, *J. geol. Soc. Lond.*, **139,** 543–554.

Tapponnier, P. & Molnar, P., 1979. Active faulting and late Cenozoic tectonics of the Tien Shan, Mongolia and Baykal region, *J. geophys. Res.*, **84,** 3425–3459.

Taymaz, T., Jackson, J. & Westaway, R., 1990. Earthquake mechanisms in the Hellenic Trench near Crete, *Geophys. J. Int.*, **102,** 695–731.

Taymaz, T., Jackson, J. & McKenzie, D., 1991. Active tectonics of the north and central Aegean Sea, *Geophys. J. Int.*, **106,** 433–490.

Valdiya, K. S., 1976. Himalayan transverse faults and folds and their parallelism with subsurface structures of north Indian plains, *Tectonophysics*, **32,** 353–386.

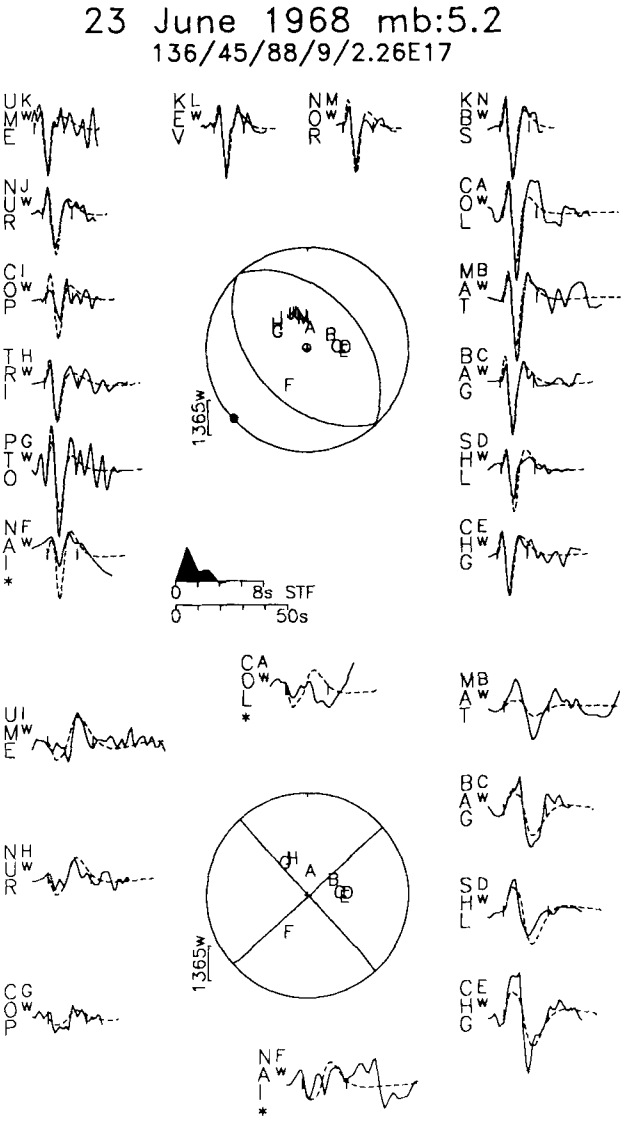

Figure A1. Minimum misfit solution for event A, on 1968 June 23. The display convention is the same as in Fig. 4. Stations marked with a '*' (e.g. NAI and COL) are not included in the inversion.

APPENDIX

1968 June 23 (event A)

This earthquake was studied by Jackson & Fitch (1981), who, on the basis of first-motion polarity data, thought that it had a fault-plane solution with a strike significantly different from the majority of Zagros reverse-faulting events. The first motion data are shown in Figs 3 and A2. Jackson & Fitch's (1981) fault-plane solution had a NE strike, and was constrained solely by the first motion polarities at the regional stations JER and KBL, which were clear and impulsive (Fig. A2). The *P* waveforms, which they also studied, were not sensitive to the strike of the reverse fault.

Our minimum misfit solution is shown in Fig. A1. *P* waveforms are abundant and clear, with the characteristic 'M' shape of a reverse fault mechanism at shallow depth. *SH* waveforms are also clear and of similar amplitude to *P*. The *SH* waveforms are not compatible with Jackson & Fitch's (1981) fault-plane solution, which must be incorrect. This is demonstrated in Fig. A2, which shows the *SH* waveforms for both the minimum misfit and Jackson & Fitch's solution. Thus, although the first motions at JER and KBL are unambiguous, they are also misleading, and incompatible with the fault orientation that is required by teleseismic waveforms. This is not especially unusual. Distortion of ray paths to regional stations can lead to their being plotted in positions on the focal sphere that are slightly incorrect. This is usually only noticeable at stations that anyway lie close to nodal planes, as in this case (see also Taymaz, Jackson & Westaway 1990; Taymaz *et al.* 1991).

The minimum misfit solution shows a simple source at a depth of 9 ± 3 km (Jackson & Fitch (1981) obtained a depth of 8 ± 4 km from *P* waveforms alone). The observed *P* waveform at NAI is apparently too small by a factor of 2. We could find no independent evidence that the station gain was wrongly recorded on the WWSSN film chip, so we simply excluded this waveform from the inversion.

The *SH* waveforms at COL and NAI were excluded from the inversion as their signal-to-noise ratio was poor. However, these two stations plot in areas of the focal sphere where there is little station coverage and we include them in this figure to show that their amplitudes are compatible with that of our solution.

We conclude that this earthquake did, after all, have a mechanism that is typical of reverse faulting events in the Zagros, with a NW strike that is parallel to the local trend of the anticlines. This fault orientation is compatible with the meisoseismal data collected in Khesht–Konar Takhteh region following this earthquake.

1971 April 6 (event B)

This was one of the smallest events (m_b 5.2) we were able to study. No *P* waveforms were large enough to model, and only six stations gave suitable *SH* waveforms (Fig. A3). The first motion readings allow for either a reverse or strike–slip faulting mechanism. Our minimum misfit solution is based on *SH* waveforms alone, and as such is compatible with either a thrust or strike–slip solution. These two solutions are plotted in the upper part of Fig. A3. The thrust solution (shown as a dashed line) is inconsistent with the first motion reading at AAE which has a very small dilatational component. Moreover, the small size of the *P* waveforms relative to *SH* suggests to us that the strike–slip solution is more likely. In Fig. A4 we compare the waveform fits of the two solutions for three stations where a *P* waveform was available. In each case we used the short-period onset time to align the synthetic as the signal was barely above the noise level. We also compare the fits of three *SH* waveforms for the two solutions. This shows that while the *SH* waveforms fit either model adequately, if this event was a thrust as Jackson & McKenzie (1984) suggested, then we would expect much larger *P* waveforms than observed. We therefore prefer the strike–slip solution. Nonetheless, this is our least-well-constrained solution, and strike is uncertain by ±25°. Depth is also difficult to constrain without *P* waveforms, and has a larger uncertainty than for the other earthquakes we studied.

1972 April 10 (event C)

This earthquake occurred NE and NW of the town of Qir (sometimes spelt Ghir), and is one of the largest events to occur in the Zagros in recent times. Ground reconnaissance (e.g. McQuillan 1973; Dewey & Grantz 1973) found no evidence of surface rupture, although a number of minor surface fissures were noted (Berberian 1976a). The

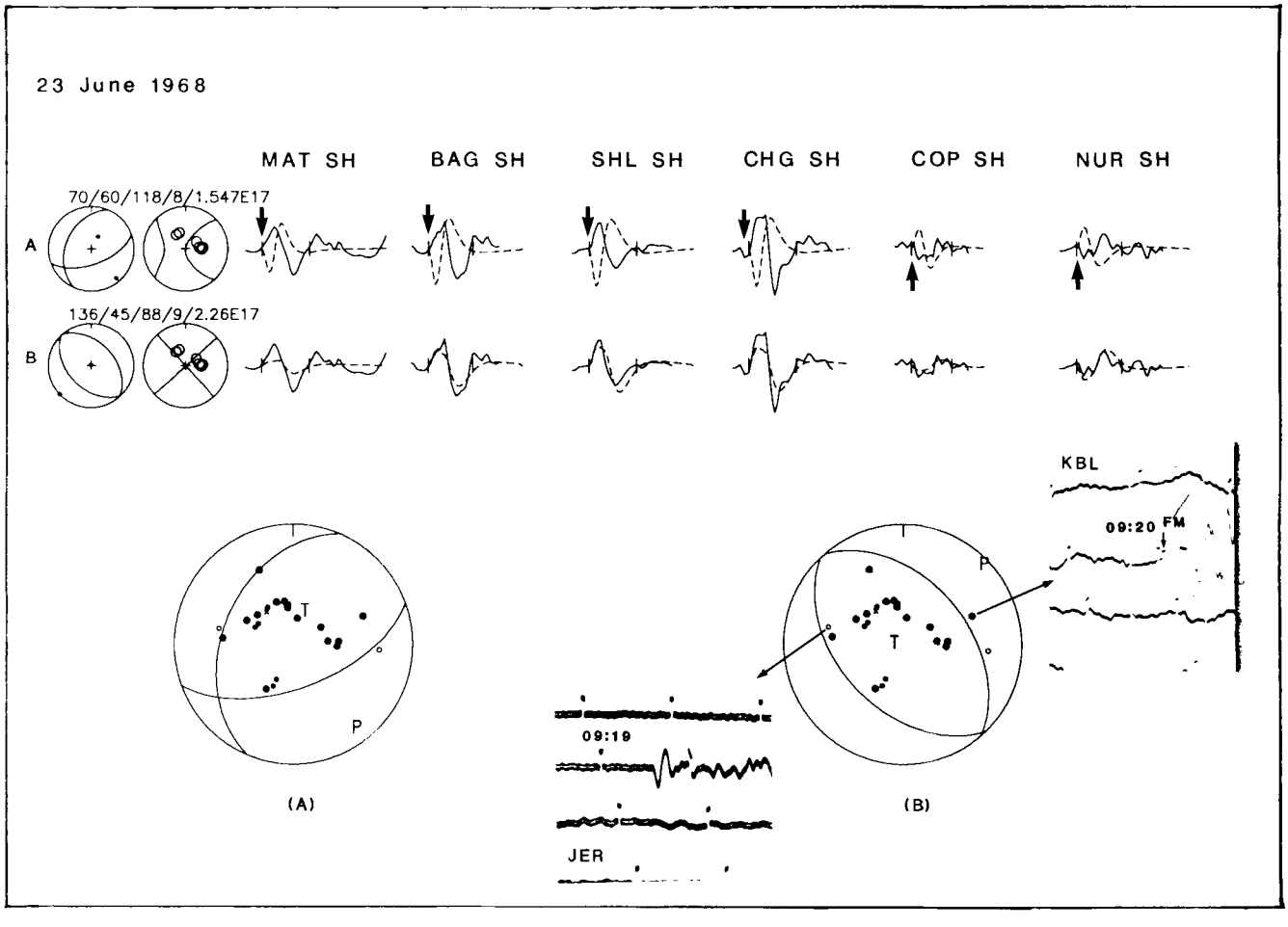

Figure A2. Comparison of the minimum misfit solution in Fig. A1 (Line A) with that obtained by Jackson & Fitch (1981) (Line B). The focal spheres in the lower half of the diagram show the first-motion readings for this event with these two solutions. The seismograms for the two stations with inconsistent first motions are shown.

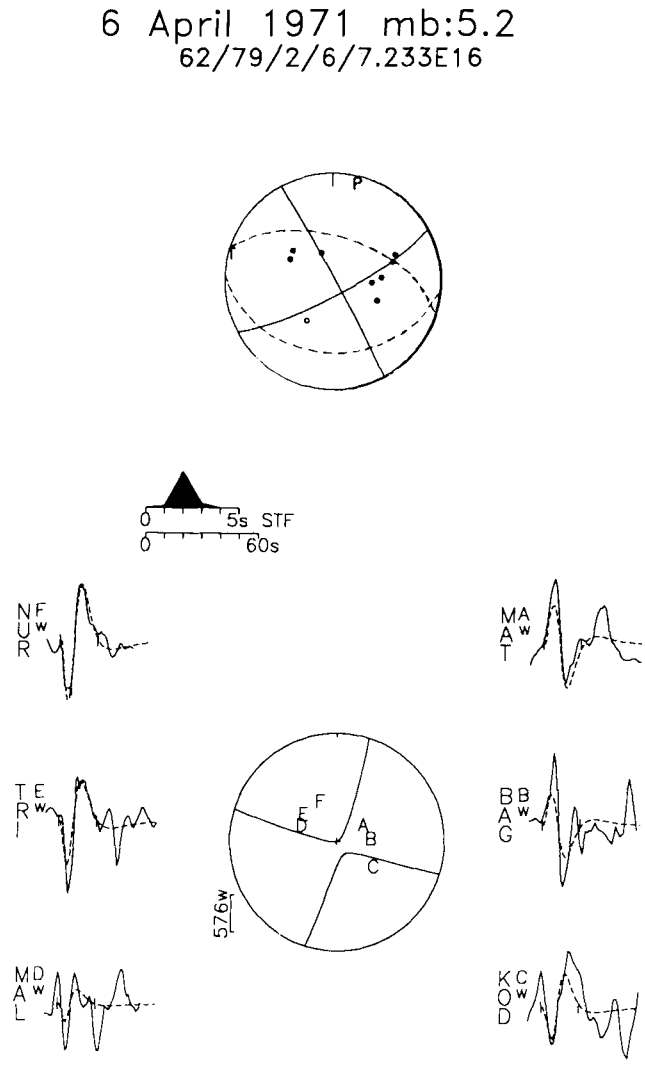

Figure A3. Minimum-misfit solution for event B (1971 April 6). The display convention is the same as in Fig. 4.

aftershock zone extended over ~40 km (Jackson & Fitch 1981). McQuillan (1973) noted that a number of anticline axes are bent in a dextral sense near the town of Quir.

Our minimum misfit solution is shown in Fig. A5. The source-time function for this earthquake was complex, and Fig. A5 shows synthetic waveforms calculated for a double event, with the second subevent 13.7 s after the first and with a different strike. The short-period seismograms of this earthquake also show an additional arrival of energy, presumably related to a second subevent, at about 14 s after the first *P* arrival. Fig. A6 shows the improved match of synthetic to observed seismograms when a second subevent is included. Line A shows a single source, which fails to match the second downswing observed in all *P* waveforms. A second subevent (line B) improves the fit noticeably. Even two subevents are insufficient to match some of the later *SH* waveforms, which show an additional pulse at between 17.5 and 20.8 s (e.g. COP, TOL, PTO and VAL): but these stations are all in the same part of the focal sphere, and this late *SH* pulse may be a path effect.

Although both subevents involved high-angle reverse faulting, the source parameters of the second are less well constrained than the first. We achieved best results when the strike of the second subevent was rotated about 34° clockwise from the first and had about half the seismic moment; but we have not attempted to estimate uncertainties in the parameters of the second subevent. The centroid depth of 9 ± 3 km for the first subevent is similar to the 12 ± 4 obtained by Jackson & Fitch (1981) from *P* waveforms alone.

1976 April 22 (event D)

This was a simple earthquake, whose source parameters are well constrained by abundant *P* and *SH* waveforms (Fig. A7). Our minimum misfit solution is inconsistent with compressional first motions at two regional stations to the NE; though both stations are close to a nodal plane (see also event A, above).

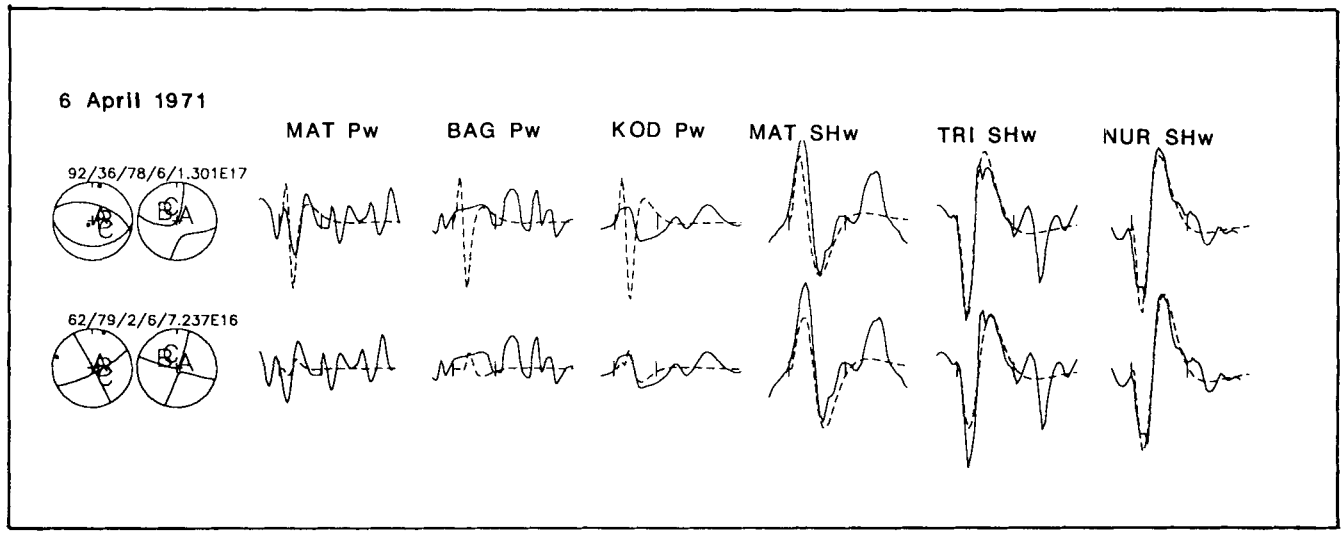

Figure A4. Comparison of thrust and strike–slip solutions for event B. While either solution provides an adequate fit to the *SH* waveforms, the small relative size of the *P* waveforms suggests the strike–slip solution is more likely.

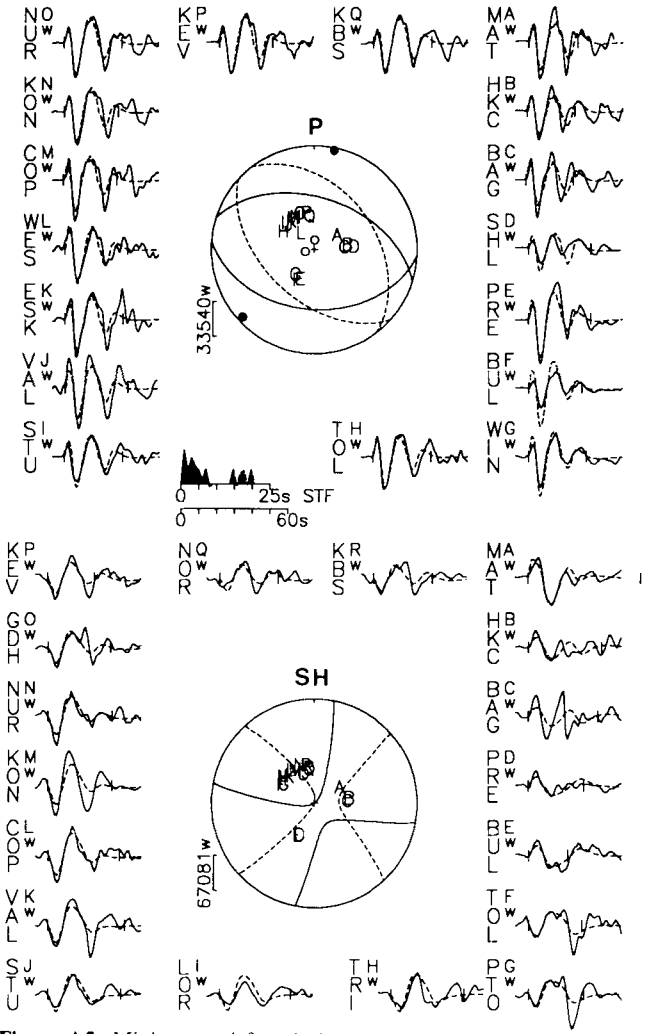

Figure A5. Minimum misfit solution for event C (1972 April 10). The display convention is the same as in Fig. 4. There are two subevents in this case. The two mechanisms are printed under the header and the second source is represented as a dashed line within the focal sphere. The source-time function shows two distinct ruptures, the second occurring 13.7 s after the onset of the first.

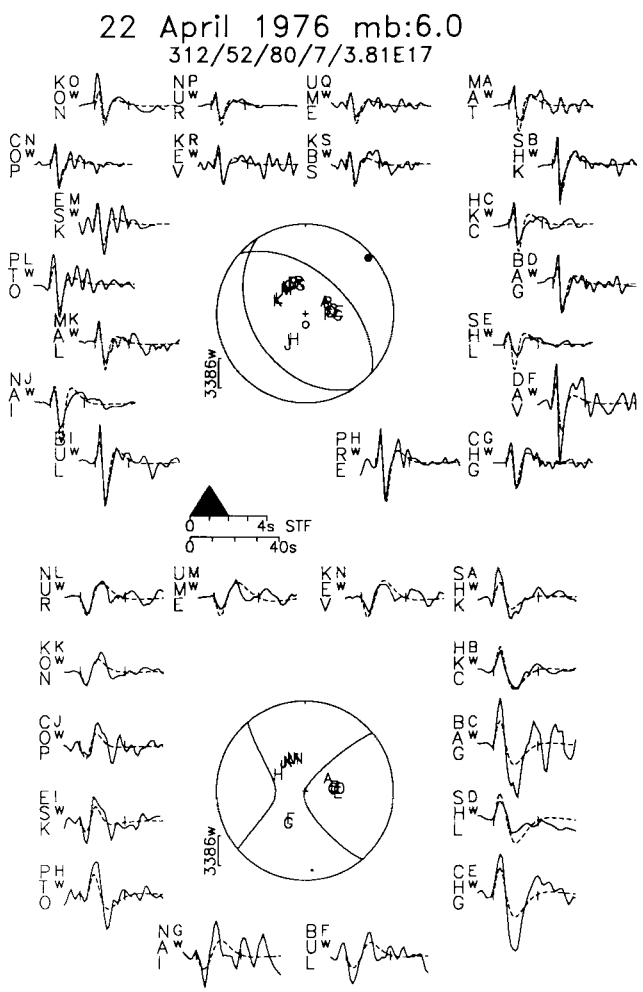

Figure A7. Minimum-misfit solution obtained for event D (1976 April 22). The display convention is the same as in Fig. 4.

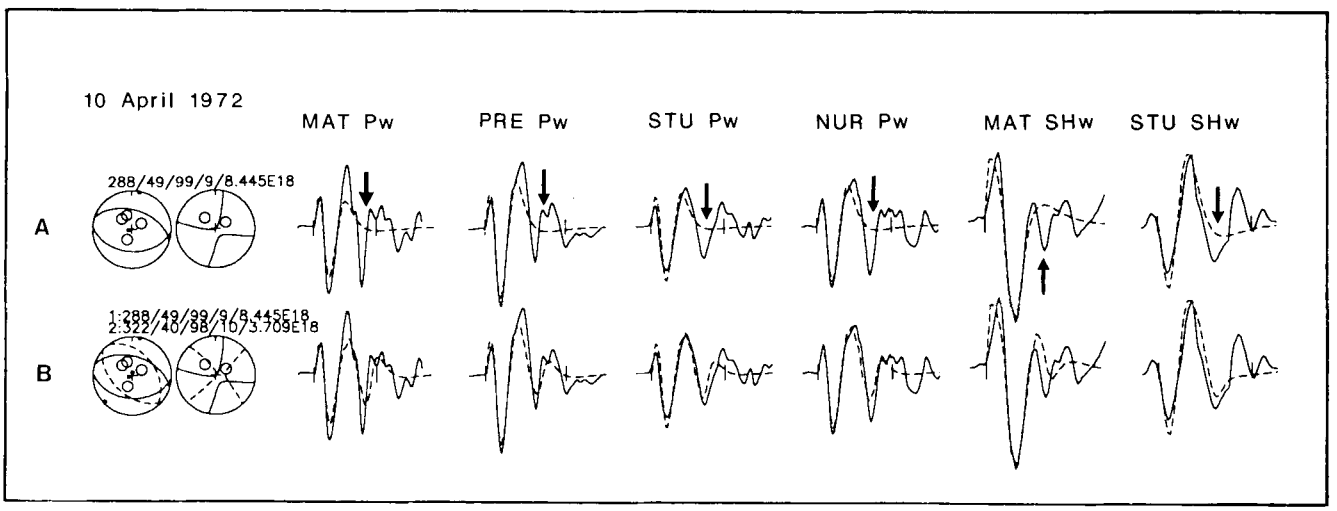

Figure A6. This figure shows the effect of each of the two subevents in Fig. A5 on the waveforms for the earthquake of 1972 April 10. Line A shows waveforms from the first subevent only. Line B shows the modifications to the waveforms when both subevents are included.

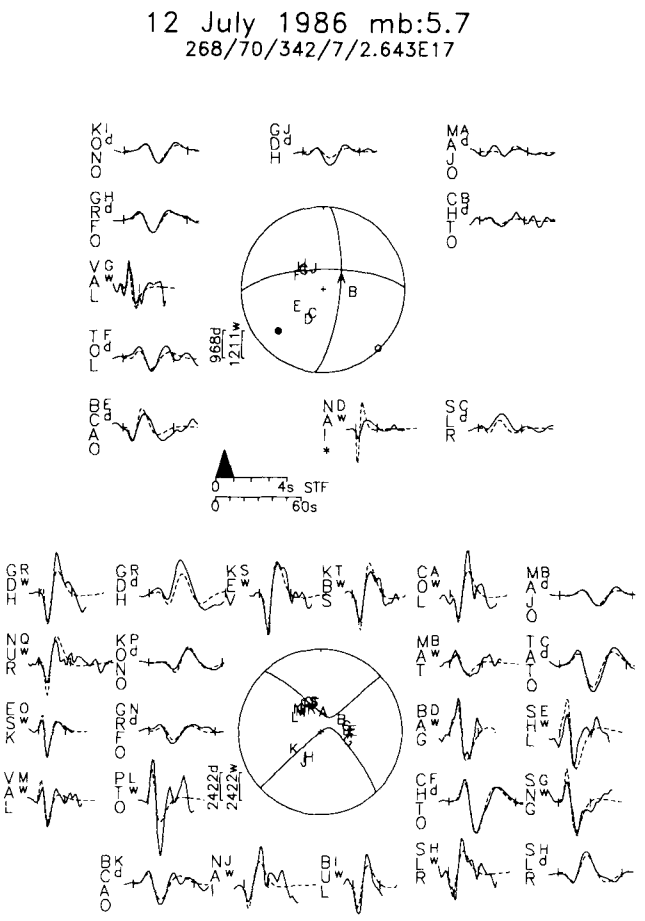

Figure A8. Minimum-misfit solution obtained for event F (1986 July 12). The display convention is the same as in Fig. 4.

1986 July 12 (event F)

First-motion polarities are not abundant for this earthquake (Fig. 3), and are consistent with either a strike–slip or reverse-fault mechanism. The small amplitudes of the *P* waveforms are, however, consistent with the strike–slip mechanism of the minimum misfit solution in Fig. A8. *SH* waveforms are particularly abundant and clear.

In Fig. A9 we compare our minimum misfit solution with two other source models. In line B the source orientation (strike, dip, rake) was held fixed at that given by the Harvard CMT solution (Dziewonski *et al.* 1987a). This solution has a similar orientation to ours, but it gives a significantly poorer fit to *SH* waveforms at SNG, VAL and ESK. In line C we show a possible reverse-faulting solution. This was obtained by starting from a reverse-fault mechanism with the same *SH* radiation pattern as our minimum misfit solution and then inverting for all source parameters. Although the inversion routine returned a reverse-fault solution, the fit to the *P* waves is noticeably poorer than for the strike–slip solution in line A. The *SH* fit is not much changed, though is marginally better at SNG. We are confident that the strike–slip solution is the correct one in this case. This agrees with observations of the meisoseismal region which lies on the Kazerun Fault and has a north–south orientation in line with this structure (M. Berberian, personal communication).

This earthquake had the shallowest centroid depth ($4^{-2}/_{+4}$ km) of the ones we studied. Depth is mainly constrained by *P* waveforms, because of their higher frequency content. In this case *P* waveforms at WWSSN stations are sparse (only VAL, NAI), but nonetheless impulsive, and suggestive of this shallow depth. Most of the digital *P* waveforms are from SRO instruments, whose narrow-band response makes them poor at resolving

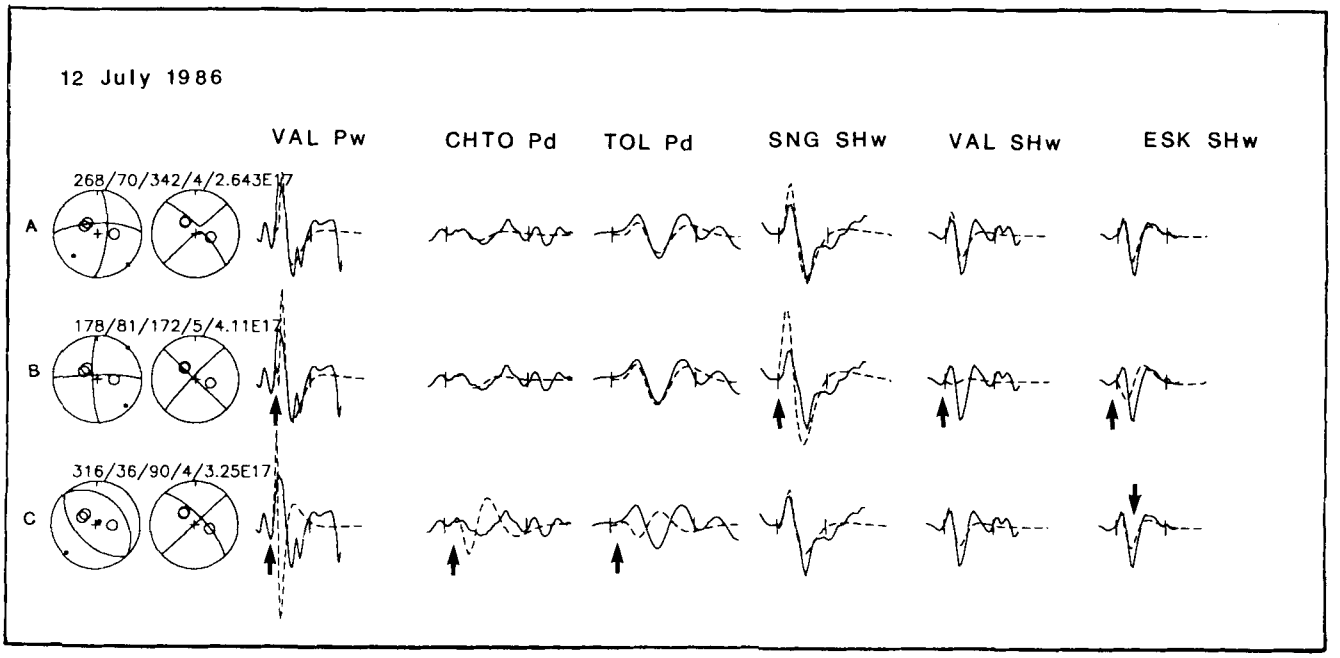

Figure A9. Comparison of solutions for event F. Line A shows our minimum-misfit solution. Line B shows the Harvard moment tensor solution. Line C is a reverse-faulting solution with a similar *SH* radiation pattern to that in line A.

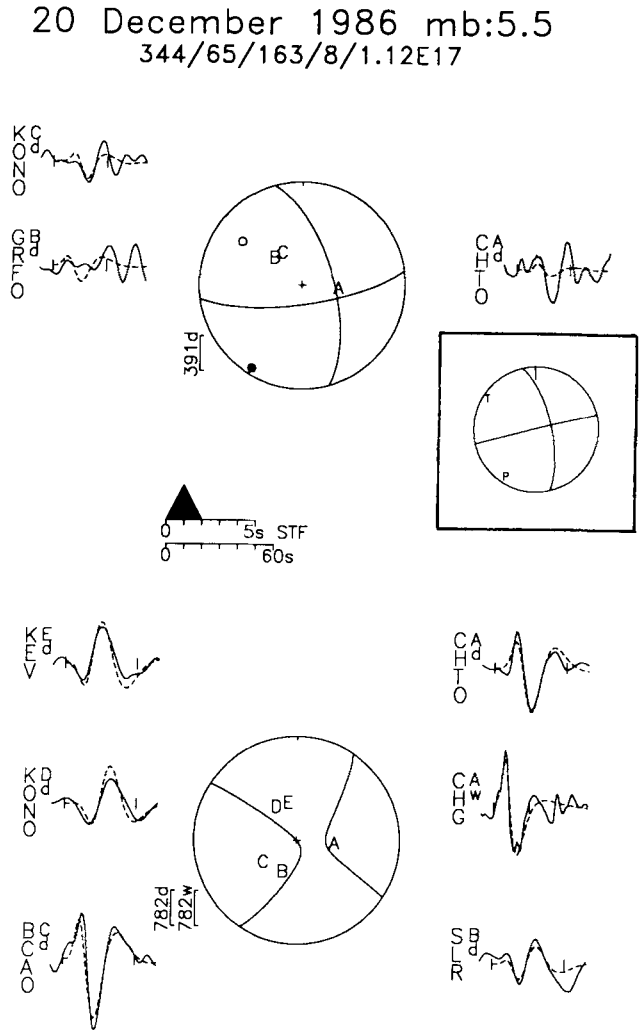

Figure A10. Minimum-misfit solution for event G (1986 December 20). The display convention is the same as in Fig. 4.

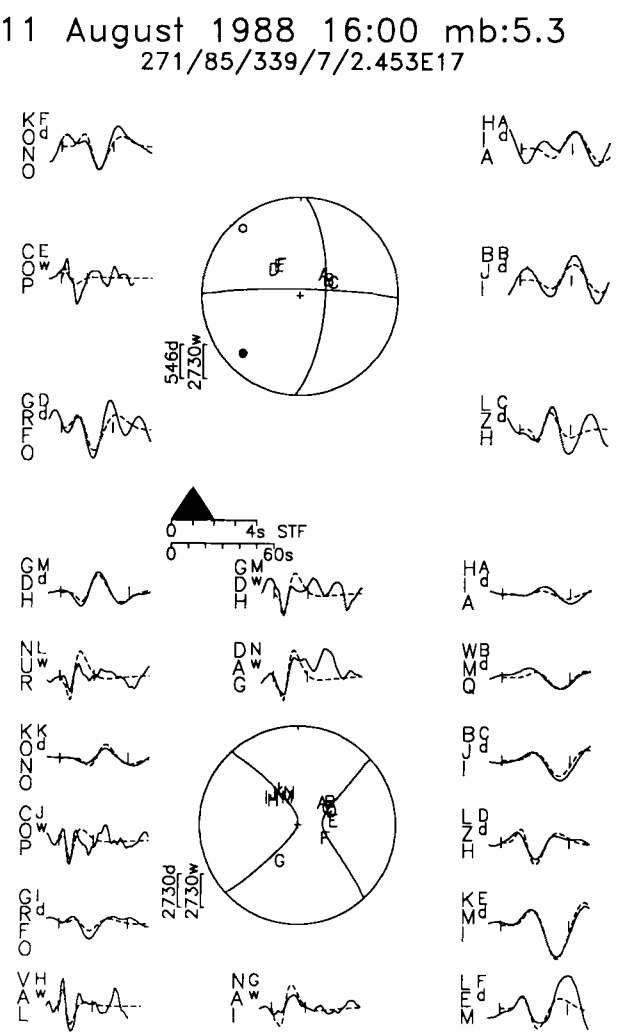

Figure A11. Minimum misfit solution for event H (1988a August 11). The display convention is the same as in Fig. 4.

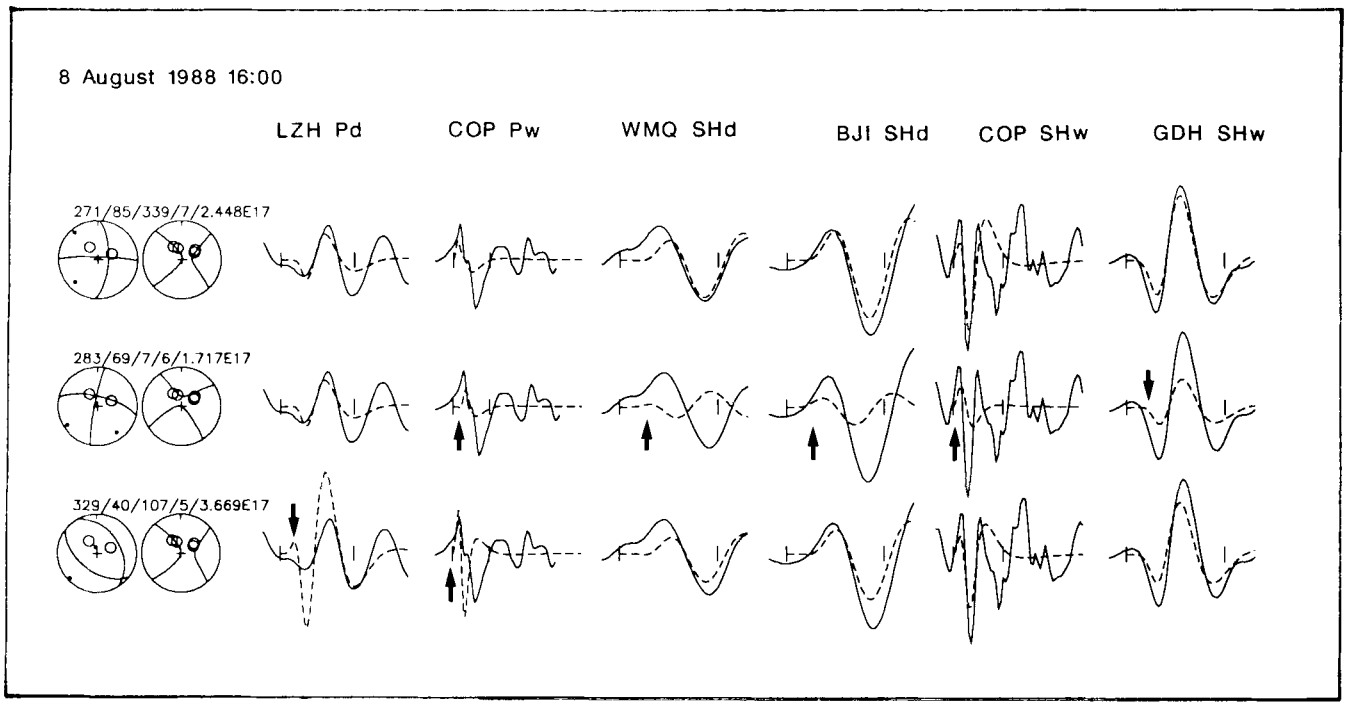

Figure A12. Comparison of models for event H. Line A shows the minimum-misfit solution. Line B shows the Harvard moment tensor solution. Line C is a reverse-faulting solution with a similar *SH* radiation pattern to that in line A.

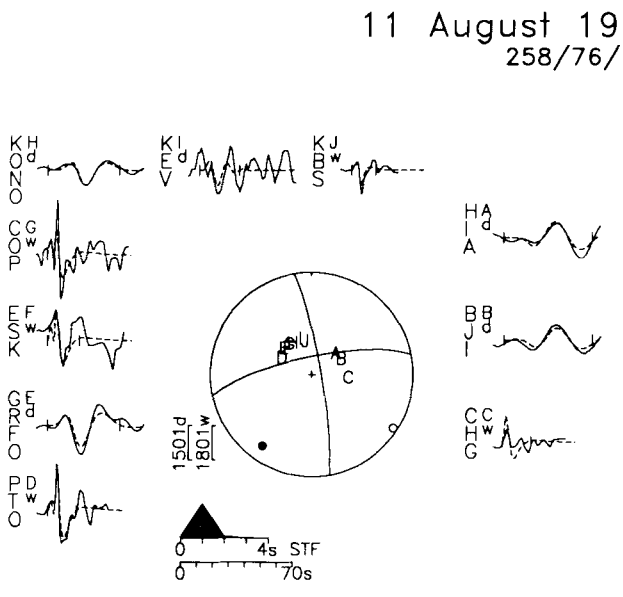

Figure A13. Minimum-misfit solution for event I (1988b August 11). The display convention is the same as in Fig. 4.

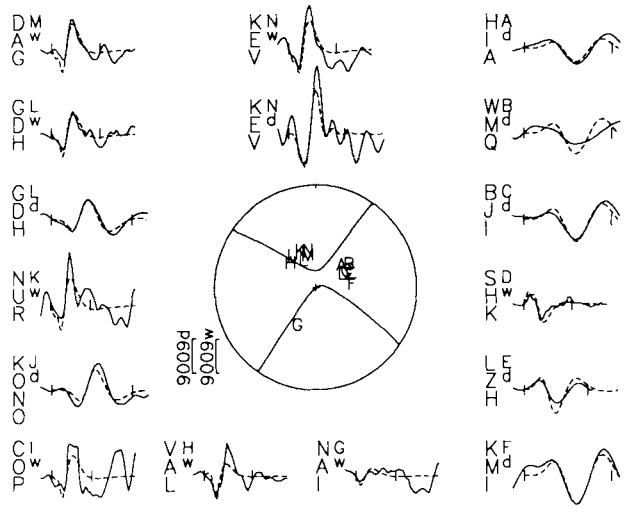

Figure A13. (*Continued*)

centroid depth. There is a suggestion that the gain at NAI was incorrectly marked on the vertical long-period WWSSN record (Fig. A8), but we can find no independent confirmation of this. Therefore it has not been included in the inversion and is marked with a '*'.

1986 December 20 (event G)

P waveforms for this event were very small compared to *SH* amplitudes, suggestive of a strike–slip mechanism. Although not many *SH* records were available, there were sufficient, with a good distribution of polarities, to constrain the *SH* nodal planes quite well (Fig. A10). *P* waves were noisy, but useful in indicating a small amplitude.

The Harvard solution for this event gives a similar strike–slip mechanism (see inset Fig. A10). This solution lies within the errors we calculate for our result. The rake in particular is poorly constrained in one direction and it is possible to obtain a reasonable fit to the *SH* waveforms for a

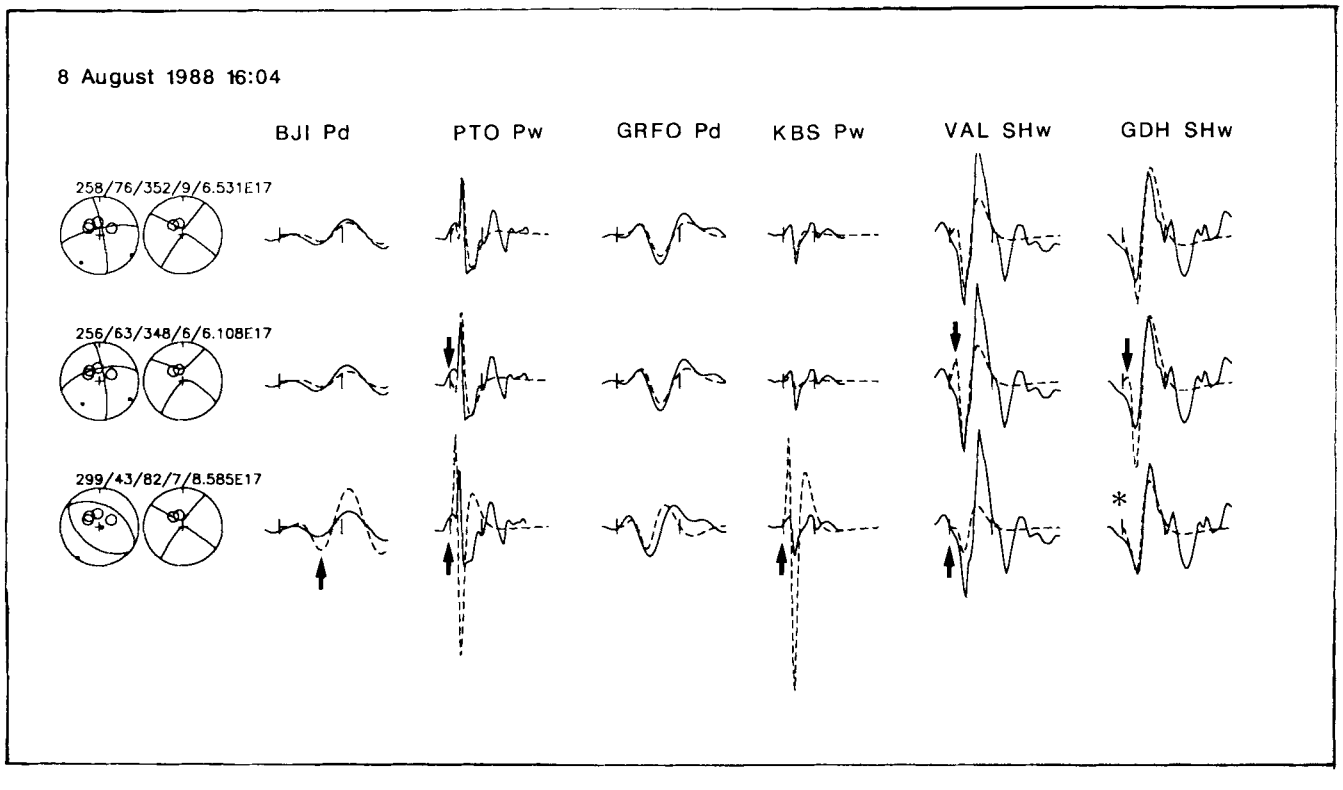

Figure A14. Comparison of models for event I. Line A shows the minimum-misfit solution. Line B shows the Harvard moment tensor solution. Line C is a reverse-faulting solution with a similar *SH* radiation pattern to that in line A.

mechanism with a larger thrust component. However, as before, the amplitudes of the *P* waveforms become unacceptably large.

1988a August 11 16:00 (event H)

This was the first of two events in this area occurring within the space of 5 min. It had a magnitude of only m_b 5.3, and generated few clear *P* waveforms. However, *SH* waveforms are abundant, and constrain those nodal planes well (Fig. A11).

In Fig. A12 we compare the minimum misfit solution of Fig. A11 (Line A) with the Harvard CMT solution (line B) and with a reverse fault that has a similar *SH* radiation pattern to our minimum misfit solution (line C), as we did in Fig. A9. The Harvard CMT solution produces a worse fit to the waveforms at several stations than does the minimum misfit solution. The reverse-fault solution produces a similar fit to the *SH* waveforms, but a worse fit to the *P* amplitude at LZH than the minimum misfit solution.

1988 August 11 16:04 (event I)

The second and larger of the two events on this day has an improved data coverage. Our minimum misfit solution is shown in Fig. A13. In Fig. A14 we compare, as before, our minimum-misfit solution with the Harvard CMT solution (line B), and with a reverse-fault mechanism with a similar *SH* radiation pattern (line C). The Harvard CMT solution is little different from our own, whereas the reverse-fault mechanism greatly overestimates the amplitudes of the *P* waveforms at PTO and KBS.

1988 December 6 (event K)

This earthquake is discussed in the main text (Fig. 4).